

# $\eta$ - $\gamma$ and $\eta'$ - $\gamma$ transition form factors in a nonlocal NJL model

D. Gómez Dumm<sup>a,b</sup>, S. Noguera<sup>c</sup> and N.N. Scoccola<sup>b,d,e</sup>

<sup>a</sup> *IFLP, CONICET – Departamento de Física, Facultad de Ciencias Exactas,  
Universidad Nacional de La Plata, C.C. 67, 1900 La Plata, Argentina*

<sup>b</sup> *CONICET, Rivadavia 1917, 1033 Buenos Aires, Argentina*

<sup>c</sup> *Departamento de Física Teórica and IFIC,  
Centro Mixto Universidad de Valencia-CSIC, E-46100 Burjassot (Valencia), Spain*

<sup>d</sup> *Physics Department, Comisión Nacional de Energía Atómica,  
Avenida del Libertador Libertador 8250, 1429 Buenos Aires, Argentina and*

<sup>e</sup> *Universidad Favaloro, Solís 453, 1078 Buenos Aires, Argentina*

## Abstract

We study the  $\eta$  and  $\eta'$  distribution amplitudes (DAs) in the context of a nonlocal  $SU(3)_L \otimes SU(3)_R$  chiral quark model. The corresponding Lagrangian allows to reproduce the phenomenological values of pseudoscalar meson masses and decay constants, as well as the momentum dependence of the quark propagator arising from lattice calculations. It is found that the obtained DAs have two symmetric maxima, which arise from new contributions generated by the nonlocal character of the interactions. These DAs are then applied to the calculation of the  $\eta$ - $\gamma$  and  $\eta'$ - $\gamma$  transition form factors. Implications of our results regarding higher twist corrections and/or contributions to the transition form factors originated by gluon-gluon components in the  $\eta$  and  $\eta'$  mesons are discussed.

## I. INTRODUCTION

In the last years, experiments carried out in B Factories have provided a large amount of data for a great variety of processes [1]. Among them, measurements of exclusive meson production, in particular,  $e^+e^- \rightarrow M e^+e^-$  and  $e^+e^- \rightarrow M \gamma$  reactions, where  $M = \pi, \eta, \eta'$ , have provided information about the photon-to-pseudoscalar meson transition form factors (TFFs),  $F_{M\gamma}(Q^2)$ , in the spacelike and timelike momentum transfer regions, respectively. High virtuality data for the pion- $\gamma$  TFF have been obtained by both BABAR [2] and BELLE [3] Collaborations, while BABAR has also measured the eta- and eta prime- $\gamma$  TFFs [4]. These data have to be added to those previously reported by the CLEO Collaboration [5] for  $\pi$ - $\gamma$ ,  $\eta$ - $\gamma$  and  $\eta'$ - $\gamma$  TFFs, as well as those obtained by the L3 Collaboration [6] for the  $\eta'$ - $\gamma$  TFF and by the CELLO Collaboration [7] for the  $\pi$ - $\gamma$  TFF.

The new experimental results have led to an intense theoretical work. In fact, from QCD it is seen that the  $M$ - $\gamma$  TFFs can be computed in terms of quark and gluon distribution amplitudes (DAs). Moreover, one can determine the corresponding asymptotic  $Q^2 \rightarrow \infty$  limits, which turn out to be model independent quantities [8, 9]. In the case of the  $\pi$ - $\gamma$  TFF, the new results —especially those from the BABAR Collaboration— indicate that  $F_{\pi\gamma}(Q^2)$  grows with  $Q^2$ , presumably crossing the asymptotic QCD limit. The implications of this exciting result have been widely discussed in the last few years (see [10–18] and references therein). On the other hand, being less controversial,  $\eta$ - $\gamma$  and  $\eta'$ - $\gamma$  TFFs have received less theoretical attention. Phenomenological studies have been carried out in Refs. [19–22], looking at the gluon content of the  $\eta$  and  $\eta'$  mesons. Other approaches have been followed in Refs. [23, 24], where the TFFs are analyzed in a model independent way through the usage of rational Padé approximants, in Ref. [25], where the anomaly sum rule is used, and in Ref. [26], where a formalism based on a chiral effective theory with two octet resonances is considered. Regarding quark model approaches, calculations have been carried out within the light front quark model [27] and, for the  $\eta$ -TFF, within the Nambu–Jona-Lasinio (NJL) model [28].

In a recent paper [13] we have studied the  $\pi$ - $\gamma$  TFF in the framework of a two-flavor version of a nonlocal NJL (nlNJL) quark model. We extend here our analysis to the case of  $\eta$ - $\gamma$  and  $\eta'$ - $\gamma$  TFFs considering a SU(3) flavor version of this nonlocal effective approach [29, 30], which represents an improvement over the local NJL model. In fact, nonlocality arises naturally in quantum field theory when the interactions involve large coupling constants. It can be seen that nonlocal form factors regularize the model in such a way that anomalies are preserved and charges are properly quantized, and there is no need to introduce extra cutoffs. Moreover, our formalism ensures the preservation of fundamental symmetries (chiral, Poincaré and local electromagnetic gauge invariances), which guarantee the proper normalization of the quark DAs.

The quark propagator is taken as one of the main ingredients of our model, the reason being that lattice QCD (LQCD) calculations allow to obtain information on this quantity directly from

the fundamental QCD theory. These calculations lead to a definite momentum dependence for both the quark mass and the quark wave function renormalization [31, 32]. Our model represents, in fact, the minimal framework that allows to incorporate the corresponding full momentum dependence by choosing adequate nonlocal form factors [33–35]. On the other hand, as it is usual in quark models, our nlNJL model neglects the explicit presence of gluons when describing the mesonic states, which are driven by their quark content. Thus, the  $\eta$  and  $\eta'$  states involve a  $q\bar{q}$  octet state (as in the case of the  $\pi$  meson) and a  $q\bar{q}$  flavor singlet state. However, one can also build up a singlet state from two gluons, and the  $q\bar{q}$  flavor singlet components in  $\eta$  and  $\eta'$  mesons will actually become mixed with the  $gg$  component by the  $Q^2$  evolution, inducing a two-gluon contribution at the leading twist order. Consequently, whereas the  $\pi$  meson state is described in the TFF calculation by a single DA, for the  $\eta$ - $\eta'$  sector one needs in general three different DAs, two of them corresponding to the quark component and one to the gluon component.

One of our objectives will be to analyze the effect of this gluon component. If we remain faithful to the philosophy of quark models, the latter has to be neglected. In that case octet and singlet states evolve in a similar way, and we can perform the  $Q^2$  evolution at next-to-leading order (NLO) to obtain the virtuality dependence of the TFFs. The quark DAs provide the dominant twist two contribution to the  $M$ - $\gamma$  TFFs, and corrections to this leading order can be introduced by considering contributions that carry extra powers of  $1/Q^2$  (we include here  $1/Q^4$  and  $1/Q^6$  terms). Therefore, in this scheme we will fix the quark DAs as well as two free parameters (coefficients of the subleading terms) in the  $M$ - $\gamma$  TFFs. Alternatively, we can assume that gluons are present already at low virtuality, which represents an additional ingredient to our model. In this second approach we will fit the lowest Gegenbauer coefficients of the gluon DA using the experimental data.

The present paper is organized as follows. In Sec. II we develop our formalism: (A) we describe the connection between  $M$ - $\gamma$  TFFs and quark DAs, (B) we present the model Lagrangian and quote our analytical results for the quark DAs, and (C) we discuss the virtuality dependence of the DAs through the evolution equations. In Sec. III we show and discuss the numerical results for the quark DAs obtained within our model for  $\pi$ ,  $\eta$  and  $\eta'$  mesons. In Sec. IV.A we analyze the results obtained for the  $\eta$ - $\gamma$  and  $\eta'$ - $\gamma$  TFFs neglecting the presence of gluons. We also show that if we assume that no gluons are present at low virtuality, the evolution equations do not generate a significant presence of gluons at higher  $Q^2$  values. Then in Sec. IV.B we analyze the effect of the presence of gluons at low virtuality on the description of the  $\eta$ - $\gamma$  and  $\eta'$ - $\gamma$  TFFs. Finally, in Sec. V we present our conclusions. Details of the calculations, including some relevant analytical expressions, can be found in Appendixes A and B.

## II. FORMALISM

### A. Theoretical framework

The transition form factors for the processes  $M \rightarrow \gamma\gamma^*$ ,  $M = \eta, \eta'$ , at large virtuality  $Q^2$  are basically determined by the quark and gluon distribution amplitudes  $\Phi_M^{(q)}$  and  $\phi_M^{(g)}$ . At the leading order in powers of  $1/Q^2$  one has

$$Q^2 F_{M\gamma}(Q^2) = \int dx \frac{1}{2} T_{q\bar{q}}(x, Q^2, \mu^2) \Phi_M^{(q)}(x, \mu^2) + \int dx \frac{1}{2} T_{gg}(x, Q^2, \mu^2) \frac{4}{3\sqrt{3}} f_M^0 \phi_M^{(g)}(x, \mu^2), \quad (1)$$

where  $f_M^0$  is a weak decay constant and  $T_{q\bar{q}}, T_{gg}$  are the amplitudes of the parton level subprocesses  $q\bar{q} \rightarrow \gamma\gamma^*$ ,  $gg \rightarrow \gamma\gamma^*$  evaluated at next-to-leading order in perturbative QCD. These are given by [20, 36, 37]

$$T_{q\bar{q}}(x, Q^2, \mu^2) = \frac{1}{x} \left\{ 1 + C_F \frac{\alpha_s(\mu)}{4\pi} \left[ \ln^2 x - \frac{x \ln x}{1-x} - 9 + (3 + 2 \ln x) \ln \frac{Q^2}{\mu^2} \right] \right\} + (x \rightarrow 1-x),$$

$$T_{gg}(x, Q^2, \mu^2) = C_F \frac{\alpha_s(\mu)}{4\pi} \frac{2 \ln x}{(1-x)^2} \left[ 3 - \frac{1}{x} - \frac{1}{2} \ln x - \ln \frac{Q^2}{\mu^2} \right] - (x \rightarrow 1-x), \quad (2)$$

where  $C_F = 4/3$  is a color group factor. As usual, we will choose the scale  $\mu^2 = Q^2$ , removing  $\ln(Q^2/\mu^2)$  terms.

The function  $\Phi_M^{(q)}(x, \mu^2)$  in Eq. (1) is given by a combination of quark DAs, which carry the soft, nonperturbative contributions to the form factor. When studying the evolution of both quark and gluon DAs it is convenient to write the operators using the  $SU(3)_F$  Gell-Mann matrices  $\lambda^i$ ,  $i = 1, \dots, 8$ , plus  $\lambda^0 = \sqrt{2/3} I$ , while to calculate the quark DAs within quark models it is usually preferable to choose a flavor basis. Thus we define the matrix  $\lambda^\ell = (\sqrt{2}\lambda^0 + \lambda^8)/\sqrt{3} = \text{diag}(1, 1, 0)$ , which is the identity in the  $(u, d)$  flavor subspace, and  $\lambda^s = \text{diag}(0, 0, \sqrt{2}) = (\lambda^0 - \sqrt{2}\lambda^8)/\sqrt{3}$ . In these two basis  $\Phi_M^{(q)}(x, \mu^2)$  is written as

$$\begin{aligned} \Phi_M^{(q)}(x, \mu^2) &= \frac{4}{3\sqrt{3}} f_M^0 \phi_M^{(q_0)}(x, \mu^2) + \frac{\sqrt{2}}{3\sqrt{3}} f_M^8 \phi_M^{(q_8)}(x, \mu^2) \\ &= \frac{5\sqrt{2}}{9} f_M^\ell \phi_M^{(q_\ell)}(x, \mu^2) + \frac{2}{9} f_M^s \phi_M^{(q_s)}(x, \mu^2), \end{aligned} \quad (3)$$

where the quark DAs are given by

$$\phi_M^{(q_i)}(x) = -\frac{i}{\sqrt{2} f_M^i} \int \frac{dz^-}{2\pi} e^{iP^+ z^- (x - \frac{1}{2})} \langle 0 | \bar{\psi}(-\frac{z}{2}) \gamma^+ \gamma_5 \lambda^i \psi(\frac{z}{2}) | M \rangle \Big|_{z^+ = \vec{z}_T = 0}, \quad (4)$$

with  $i = 0, 8$  or  $i = \ell, s$ , depending on the basis choice. We use here light-front spacetime coordinates  $x^\pm = (x^0 \pm x^3)/\sqrt{2}$ ,  $\vec{x}_T = (x^1, x^2)$ . The meson weak decay constants  $f_M^i$  are defined by

$$f_M^i = \frac{1}{i\sqrt{2}P^+} \langle 0 | \bar{\psi}(0) \gamma^+ \gamma_5 \lambda^i \psi(0) | M \rangle, \quad (5)$$

thus it is easy to see that the quark DAs satisfy the sum rule

$$\int_0^1 dx \phi_M^{(q_i)}(x) = 1 \quad (6)$$

for any scale  $\mu$ . Moreover, the quark DAs are symmetric under the change  $x \rightarrow (1-x)$ . Finally, the gluon DA in Eq. (1) is given by

$$\phi_M^{(g)}(x) = \frac{2}{\sqrt{3} f_M^0} \frac{1}{P^+} \int \frac{dz^-}{2\pi} e^{iP^+ z^- (x - \frac{1}{2})} n_\mu n_\nu \langle 0 | G^{\mu\alpha}(-\frac{z}{2}) \tilde{G}_\alpha^\nu(\frac{z}{2}) | P \rangle \Big|_{z^+ = \vec{z}_T = 0} , \quad (7)$$

where  $G^{\mu\nu}$  is the gluon field strength tensor and  $\tilde{G}^{\mu\nu} = \frac{1}{2} \epsilon^{\mu\nu\alpha\beta} G_{\alpha\beta}$ . Notice that  $\phi_M^{(g)}(x)$  is antisymmetric under the change  $x \rightarrow (1-x)$ , hence

$$\int_0^1 dx \phi_M^{(g)}(x) = 0 ,$$

and there is no natural way to normalize the gluon DA. The prefactor present in Eq. (7) is just a convention, and other definitions can be found in literature (see the discussion in Ref. [20]). A change in this prefactor can be compensated through a factor into the integrand in the second term of Eq. (1).

In the case of the  $\pi \rightarrow \gamma\gamma^*$  TFF the situation is simpler, since there is no singlet contribution. One has

$$Q^2 F_{\pi\gamma}(Q^2) = \frac{\sqrt{2}}{3} f_\pi \int dx \frac{1}{2} T_{q\bar{q}}(x) \phi_\pi(x, \mu^2) , \quad (8)$$

where the pion DA is given by

$$\phi_\pi(x) = \frac{-i}{\sqrt{2} f_\pi} \int \frac{dz^-}{2\pi} e^{iP^+ z^- (x - \frac{1}{2})} \langle 0 | \bar{\psi}(-\frac{z}{2}) \gamma^+ \gamma_5 \lambda^3 \psi(\frac{z}{2}) | \pi \rangle \Big|_{z^+ = \vec{z}_T = 0} . \quad (9)$$

## B. Neutral pseudoscalar meson distribution amplitudes in a nonlocal NJL model

We consider here the meson DAs within a nonlocal NJL (nlNJL) model. The corresponding Euclidean effective action, in the case of  $SU(3)_F$  flavor symmetry, is given by [30]

$$S_E = \int d^4x \left\{ \bar{\psi}(x)(-i\not{\partial} + \hat{m})\psi(x) - \frac{G}{2} [j_a^S(x)j_a^S(x) + j_a^P(x)j_a^P(x) + j^r(x)j^r(x)] \right. \\ \left. - \frac{H}{4} A_{abc} [j_a^S(x)j_b^S(x)j_c^S(x) - 3j_a^S(x)j_b^P(x)j_c^P(x)] \right\} , \quad (10)$$

where  $\psi(x)$  is the  $SU(3)_F$  fermion triplet  $\psi = (u \ d \ s)^T$ , and  $\hat{m} = \text{diag}(m_u, m_d, m_s)$  is the current quark mass matrix. We will work in the isospin symmetry limit, assuming  $m_u = m_d$ . The model includes flavor mixing through the 't Hooft-like term driven by  $H$ , where the constants  $A_{abc}$  are defined by

$$A_{abc} = \frac{1}{3!} \epsilon_{ijk} \epsilon_{mnl} (\lambda^a)_{im} (\lambda^b)_{jn} (\lambda^c)_{kl} , \quad (11)$$

with  $a = 0, \dots, 8$ . The fermion currents are given by

$$\begin{aligned} j_a^s(x) &= \int d^4z \mathcal{G}(z) \bar{\psi} \left( x + \frac{z}{2} \right) \lambda^a \psi \left( x - \frac{z}{2} \right) , \\ j_a^p(x) &= \int d^4z \mathcal{G}(z) \bar{\psi} \left( x + \frac{z}{2} \right) i \lambda^a \gamma_5 \psi \left( x - \frac{z}{2} \right) , \\ j^r(x) &= \int d^4z \mathcal{F}(z) \bar{\psi} \left( x + \frac{z}{2} \right) \frac{\overleftrightarrow{\not{D}}}{2\kappa} \psi \left( x - \frac{z}{2} \right) , \end{aligned} \quad (12)$$

where the functions  $\mathcal{G}(z)$  and  $\mathcal{F}(z)$  are covariant form factors responsible for the nonlocal character of the interactions. Notice that the relative weight of the interaction driven by  $j^r(x)$ , which leads to quark wave function renormalization, is controlled by the parameter  $\kappa$ . In the mean field approximation (MFA), which will be used here in what follows, the quark propagator for each flavor  $f = u, d, s$  can be expressed as

$$S_f(p) = \frac{Z(p)}{-\not{p} + M_f(p)} , \quad (13)$$

where  $M_f(p)$  and  $Z(p)$  stand for momentum dependent effective mass and wave function renormalization (WFR), respectively. One has [30]

$$M_f(p) = Z(p) \left[ m_f + \bar{\sigma}_f g(p) \right] , \quad Z(p) = \left[ 1 - \frac{\bar{\zeta}}{\kappa} f(p) \right]^{-1} , \quad (14)$$

where  $g(p)$  and  $f(p)$  are Fourier transforms of  $\mathcal{G}(z)$  and  $\mathcal{F}(z)$ , while  $\bar{\sigma}_f$  and  $\bar{\zeta}$  are mean field values of scalar fields associated with the corresponding currents in Eq. (12). Details of the procedure carried out to obtain these quantities are given in App. A.

The momentum dependence of the interaction form factors can be now obtained from lattice QCD results. Following the analysis in Ref. [32], the effective mass  $M_u(p)$  can be written as

$$M_u(p) = m_u + \alpha_m f_m(p) , \quad (15)$$

where

$$f_m(p) = 1 / \left[ 1 + (p^2 / \Lambda_0^2)^\alpha \right] , \quad (16)$$

with  $\alpha = 3/2$ . From Eqs. (14) one has then  $\alpha_m = (m_u \bar{\zeta} / \kappa + \bar{\sigma}_u) / (1 - \bar{\zeta} / \kappa)$ . For the wave function renormalization we use the parametrization [33, 35]

$$Z(p) = 1 - \alpha_z f_z(p) , \quad (17)$$

where

$$f_z(p) = 1 / \left( 1 + p^2 / \Lambda_1^2 \right)^{5/2} . \quad (18)$$

Here the new parameter  $\alpha_z$  is given by  $\alpha_z = -\bar{\zeta} / (\kappa - \bar{\zeta})$ . The functions  $f(p)$  and  $g(p)$  can be now easily obtained from Eqs. (14-18). As shown in Refs. [33, 35], for an adequate choice of parameters

these functional forms can reproduce very well the momentum dependence of quark mass and WFR obtained in lattice calculations. We complete the model parameter fixing by taking as phenomenological inputs the values of the pion, kaon and  $\eta'$  masses and the pion weak decay constant [30]. The resulting model parameters are given in Table I.

$m_u$ (MeV)	$m_s$ (MeV)	$G\Lambda_0^2$	$-H\Lambda_0^5$	$\kappa/\Lambda_0$	$\Lambda_0$ (GeV)	$\Lambda_1$ (GeV)
2.6	64.9	16.65	202.8	10.34	0.795	1.510

TABLE I: Model parameters

Given this effective model for the strong interactions at low energies, one can explicitly evaluate the quark DAs from Eq. (4). Since the amplitude involves a bilocal axial vector current, one should introduce into the effective action in Eq. (10) a coupling to an external axial gauge field  $\mathcal{A}_\mu^a$ . For a local theory this can be done just through the replacement

$$\partial_\mu \rightarrow \partial_\mu + i \gamma_5 \lambda^a \mathcal{A}_\mu^a(y) . \quad (19)$$

In the case of the above described nonlocal model, however, the situation is more complicated since the inclusion of gauge interactions implies a change not only in the kinetic piece of the Lagrangian but also in the nonlocal currents appearing in the interaction terms. If  $x$  and  $z$  denote the space variables in the definitions of the nonlocal currents [see Eq. (12)], one has

$$\begin{aligned} \psi(x - z/2) &\rightarrow W(x, x - z/2) \psi(x - z/2) , \\ \psi^\dagger(x + z/2) &\rightarrow \psi^\dagger(x + z/2) W(x + z/2, x) . \end{aligned} \quad (20)$$

Here the function  $W(s, t)$  is defined by

$$W(s, t) = \text{P exp} \left[ i \int_s^t dr_\mu \gamma_5 \lambda^a \mathcal{A}_\mu^a(r) \right] , \quad (21)$$

where  $r$  runs over an arbitrary path connecting  $s$  with  $t$ .

This procedure has been analyzed in detail within nlNJL models, in particular regarding the calculation of the pseudoscalar meson decay constants [29, 33, 38], see Eq. (5). The situation is similar for the case of the bilocal axial current in the definition of the meson DA. In fact, the basic physical idea beyond the factorization of the meson TFF into hard and soft contributions is that for high  $Q^2$  the struck quark loses its high momentum before being able to interact with the remaining quarks and gluons of the hadron ( $Q^2 \sim 1 \text{ GeV}^2$  implies a time scale of the order of  $10^{-24} \text{ s}$ ). Therefore, the nonlocal interaction does not see the struck quark but only the quarks in the hadron before and after the photon absorption-emission process. This can be effectively implemented by introducing an external fictitious probe carrying the adequate quantum numbers, which in our case

is a gauge axial field (a similar situation has been studied in the case of the pion parton distribution, see Refs. [33, 34]). Thus, the axial vertex in Eq. (4) will become dressed by the nonlocal interaction, irrespective of whether the quark current is a local or a bilocal one (as in this case).

The steps to be followed in the explicit calculation of the quark DA within the nlNJL model are detailed in Appendix A. We quote here the resulting expression. In the flavor basis (i.e.  $q_i = q_\ell, q_s$ ) we have

$$\phi_M^{(q_i)}(x) = \frac{2\sqrt{2} N_c g_{Mqq}}{f_M^i} \int \frac{dw d^2 k_T}{(2\pi)^4} F_i(w, x, k_T) , \quad (22)$$

where  $g_{Mqq}$  stands for an effective quark-meson coupling constant [see Eq. (59) in Appendix A] and the integration variables are related to the meson and quark Euclidean four-momentum  $P$  and  $k$ , respectively. Considering the light front variables in the frame where the transverse component  $\vec{P}_T$  vanishes, the invariants  $k^2$  and  $k \cdot P$  can be written in terms of the variables  $w$  and  $k_T$  as

$$k^2 = -i w \left( x - \frac{1}{2} \right) + m_M^2 \left( x - \frac{1}{2} \right)^2 + k_T^2 , \quad k \cdot P = -i \frac{w}{2} .$$

It is convenient to separate the integrand in Eq. (22) into two pieces,

$$F_i(w, x, k_T) = F_i^{(1)}(w, x, k_T) + F_i^{(2)}(w, x, k_T) . \quad (23)$$

The explicit expressions for these functions are

$$F_i^{(1)}(w, x, k_T) = \frac{g(k)}{2} \frac{Z(k_+) Z(k_-)}{D_i(k_+) D_i(k_-)} \left[ \frac{1}{Z(k_+)} + \frac{1}{Z(k_-)} \right] [(1-x) M_i(k_+) + x M_i(k_-)] , \quad (24)$$

$$\begin{aligned} F_i^{(2)}(w, x, k_T) = & g(k) \frac{Z(k_+) Z(k_-)}{D_i(k_+) D_i(k_-)} \left\{ [k_+ \cdot k_- + M_i(k_+) M_i(k_-)] \nu_i^{(1)} \right. \\ & \left. - k \cdot [k_+ M_i(k_-) - k_- M_i(k_+)] \nu_i^{(2)} \right\} - \frac{M_i(k) Z(k)}{D_i(k) \bar{\sigma}_i} \nu_i^{(1)} , \end{aligned} \quad (25)$$

where  $M_\ell = M_u = M_d$  and  $\bar{\sigma}_\ell = \bar{\sigma}_u = \bar{\sigma}_d$ . We have defined  $k_\pm = k \pm P/2$  and  $D_i(k) = k^2 + M_i(k)^2$ , while the functions  $\nu_i^{(1)}$  and  $\nu_i^{(2)}$  in  $F_i^{(2)}$  are given by

$$\begin{aligned} \nu_i^{(1)} &= \frac{(x - \frac{1}{2})}{k \cdot P} \left[ \frac{M_i(k_+)}{Z(k_+)} + \frac{M_i(k_-)}{Z(k_-)} - 2 \frac{M_i(k)}{Z(k)} + m_M^2 \bar{\sigma}_i \alpha_g^- \right] + \bar{\sigma}_i \alpha_g^- , \\ \nu_i^{(2)} &= \frac{(x - \frac{1}{2})}{k \cdot P} \left[ \frac{1}{Z(k_-)} - \frac{1}{Z(k_+)} + m_M^2 \bar{\zeta} \alpha_f^+ \right] + \bar{\zeta} \alpha_f^+ . \end{aligned} \quad (26)$$

Here  $\alpha_g^-$  and  $\alpha_f^+$  depend in general on the integration path in Eq. (21). For a straight line path one has

$$\begin{aligned} \alpha_g^- &= \int_0^1 d\lambda \frac{\lambda}{2} g'(k - \lambda P/2) - \int_{-1}^0 d\lambda \frac{\lambda}{2} g'(k - \lambda P/2) , \\ \alpha_f^+ &= \int_{-1}^1 d\lambda \frac{\lambda}{2} f'(k - \lambda P/2) , \end{aligned} \quad (27)$$

where  $g'(k) \equiv dg(k)/dk^2$ , and same for  $f'(k)$ .



It is important to mention that, even when our effective model leads to an adequate phenomenological pattern for low energy meson phenomenology, there are some differences between model predictions and phenomenological values of the  $\eta$  and  $\eta'$  decay constants (see Table XII in App. A). In our numerical calculations, when evaluating the  $\eta$  and  $\eta'$  DAs from Eq. (22) we will take the values of  $f_M^i$  arising from our model, in order to guarantee the proper normalization condition Eq. (6). On the other hand, we will use the phenomenological values for  $f_M^\ell$  or  $f_M^s$  when evaluating the flavor mixing leading to the quark DAs, Eq. (3).

### C. Distribution amplitude evolution

Let us analyze the evolution of the DAs with the energy scale. Firstly, notice that QCD evolution equations mix the  $q\bar{q}$  singlet flavor component with the  $gg$  component in  $\eta$  and  $\eta'$  DAs. Consequently, after obtaining the low energy  $q\bar{q}$  flavor DAs  $\phi_M^{(qi)}$ ,  $i = \ell, s$ , from the effective quark model, it is convenient to change to the octet and singlet DAs

$$\begin{aligned}\phi_M^{(qs)}(x) &= \frac{1}{\sqrt{3} f_M^8} \left[ f_M^\ell \phi_M^{(q\ell)}(x) - \sqrt{2} f_M^s \phi_M^{(qs)}(x) \right], \\ \phi_M^{(q0)}(x) &= \frac{1}{\sqrt{3} f_M^0} \left[ \sqrt{2} f_M^\ell \phi_M^{(q\ell)}(x) + f_M^s \phi_M^{(qs)}(x) \right].\end{aligned}\quad (28)$$

Once the latter are known at a given  $\mu_0$  scale, their evolution up to a higher scale  $\mu$  can be obtained from perturbative QCD. In order to study this evolution it is convenient to expand the DAs in series of Gegenbauer polynomials:

$$\begin{aligned}\phi_M^{(qi)}(x, \mu) &= 6x(1-x) \sum_{n=0,2,4,\dots} a_{Mn}^{(qi)}(\mu) C_n^{3/2}(2x-1), \\ \phi_M^{(g)}(x, \mu) &= x^2(1-x)^2 \sum_{n=2,4,\dots} a_{Mn}^{(g)}(\mu) C_{n-1}^{5/2}(2x-1),\end{aligned}\quad (29)$$

where  $i = 0, 8$ , and we have now explicitly denoted the  $\mu$  dependence of the DAs. Notice that only  $n$ -even terms contribute to the sums, due to the symmetric (antisymmetric) behavior of the quark DAs (gluon DA) under the replacement  $x \leftrightarrow 1-x$ . Moreover, since  $\phi_M^{(qi)}(x, \mu)$  ( $i = 0, 8$ ) satisfy the sum rule Eq. (6), the first coefficients  $a_{M0}^{(q0)}(\mu)$  and  $a_{M0}^{(qs)}(\mu)$  have to be equal to 1 for any value of  $\mu$ . Thus, all the information from the meson effective model is included in the remaining coefficients  $a_{Mn}^{(qi)}(\mu)$  and  $a_{Mn}^{(g)}(\mu)$ , with  $n = 2, 4, \dots$ .

From the orthogonality relations satisfied by the Gegenbauer polynomials one can obtain the coefficients at the  $\mu_0$  scale, namely

$$a_{Mn}^{(qi)}(\mu_0) = \frac{2(2n+3)}{3(n+1)(n+2)} \int_0^1 dx C_n^{3/2}(2x-1) \phi_M^{(qi)}(x, \mu_0), \quad (30)$$

$$a_{Mn}^{(g)}(\mu_0) = \frac{144(2n+5)}{(n+1)(n+2)(n+3)(n+4)} \int_0^1 dx C_{n-1}^{5/2}(2x-1) \phi_M^{(g)}(x, \mu_0). \quad (31)$$

Notice that Eq. (30) holds either if one is working in the flavor basis ( $i = \ell, s$ ) or in the  $SU(3)_F$  basis ( $i = 0, 8$ ). At the LO the Gegenbauer polynomials are eigenfunctions of the evolution kernel, therefore  $a_{Mn}$  coefficients of different order  $n$  do not mix with each other [21]. On the other hand, as stated, QCD evolution equations mix the gluon and singlet quark components for  $n \geq 2$ . The evolution of these coefficients up to a scale  $\mu$  is given by (see Refs. [20, 21])

$$\begin{aligned} a_{Mn}^{(q_0)}(\mu) &= a_{Mn}^{(+)}(\mu_0) \left( \frac{\alpha_s(\mu_0)}{\alpha_s(\mu)} \right)^{\gamma_n^{(+)} / \beta_0} + \rho_n^{(-)} a_{Mn}^{(-)}(\mu_0) \left( \frac{\alpha_s(\mu_0)}{\alpha_s(\mu)} \right)^{\gamma_n^{(-)} / \beta_0}, \\ a_{Mn}^{(g)}(\mu) &= \rho_n^{(+)} a_{Mn}^{(+)}(\mu_0) \left( \frac{\alpha_s(\mu_0)}{\alpha_s(\mu)} \right)^{\gamma_n^{(+)} / \beta_0} + a_{Mn}^{(-)}(\mu_0) \left( \frac{\alpha_s(\mu_0)}{\alpha_s(\mu)} \right)^{\gamma_n^{(-)} / \beta_0}. \end{aligned} \quad (32)$$

Here  $\beta_0 = 11 - 2n_f/3$ ,  $n_f$  being the number of active flavors at the scale of the process (in our case we take  $n_f = 4$ ), and  $\gamma_n^{(\pm)}$  are the eigenvalues of the anomalous dimension matrix  $\gamma_n$ . These are given by

$$\gamma_n^{(\pm)} = \frac{1}{2} \left[ \gamma_n^{qq} + \gamma_n^{gg} \pm \sqrt{(\gamma_n^{qq} - \gamma_n^{gg})^2 + 4 \gamma_n^{qg} \gamma_n^{gq}} \right], \quad (33)$$

where the (LO) matrix elements of  $\gamma_n$  read

$$\begin{aligned} \gamma_n^{qq} &= C_F \left[ 3 + \frac{2}{(n+1)(n+2)} - 4 \sum_{i=1}^{n+1} \frac{1}{i} \right], \\ \gamma_n^{qg} &= C_F \frac{n(n+3)}{3(n+1)(n+2)}, \\ \gamma_n^{gq} &= \frac{36}{(n+1)(n+2)}, \\ \gamma_n^{gg} &= \beta_0 + N_c \left[ \frac{8}{(n+1)(n+2)} - 4 \sum_{i=1}^{n+1} \frac{1}{i} \right]. \end{aligned} \quad (34)$$

The coefficients  $\rho_n^{(+)}$  and  $\rho_n^{(-)}$ , which weight the presence of quarks in the gluon DA and gluons in the singlet quark DA, respectively, are given by

$$\begin{aligned} \rho_n^{(+)} &= 6 \frac{\gamma_n^{qg}}{\gamma_n^{(+)} - \gamma_n^{gg}}, \\ \rho_n^{(-)} &= \frac{1}{6} \frac{\gamma_n^{gq}}{\gamma_n^{(-)} - \gamma_n^{qq}}. \end{aligned} \quad (35)$$

Finally, the evolution of the strong coupling constant  $\alpha_s$  at the LO is given by

$$\alpha_s(\mu) = \frac{4\pi}{\beta_0 \ln(\mu^2/\Lambda^2)}, \quad (36)$$

with  $\Lambda = 0.224$  GeV.

In Table II we quote the values of the anomalous dimensions for the first values of  $n$ . Already for  $n = 2$  it is seen that  $\gamma^{(+)}$  and  $\gamma^{(-)}$  are close to  $\gamma^{qq}$  and  $\gamma^{gg}$ , respectively, and the differences become even smaller for larger  $n$ . The numerical values for  $\rho^{(\pm)}$  and the product  $\rho_n^{(+)} \rho_n^{(-)}$  for the first values of  $n$  are given in Table III.

$n$	2	4	6	8	10	Asymptotic form
$\gamma_n^{(+)}$	-5.379	-8.040	-9.759	-11.046	-12.078	$-\frac{16}{3} \ln n$
$\gamma_n^{(-)}$	-11.84	-18.32	-22.37	-25.36	-27.73	$-12 \ln n$
$\gamma_n^{qq}$	-5.556	-8.089	-9.781	-11.06	-12.09	$-\frac{16}{3} \ln n$
$\gamma_n^{gg}$	-11.67	-18.27	-22.35	-25.35	-27.72	$-12 \ln n$

TABLE II: Numerical values of the first  $\gamma_n^{(\pm)}$ ,  $\gamma_n^{qq}$  and  $\gamma_n^{gg}$  coefficients, and asymptotic values.

$n$	2	4	6	8	10	Asymptotic form
$\rho_n^{(+)}$	2.8627	0.7041	0.3063	0.1678	0.1045	$162/(5 n^2 \ln n)$
$\rho_n^{(-)}$	-0.0098	-0.0068	-0.0057	-0.0051	-0.0047	$-1/(90 \ln n)$
$\rho_n^{(+)} \rho_n^{(-)}$	-0.0281	-0.0048	-0.0017	-0.0008	-0.0005	$-9/(25 n^2 \ln^2 n)$

TABLE III: Numerical values of the first  $\rho_n^{(\pm)}$  coefficients, and asymptotic values.

In the case of the distribution amplitude  $\phi_M^{(qs)}$ , at the LO the evolution is just governed by the anomalous dimension  $\gamma_n^{qq}$ . One has

$$a_{Mn}^{(qs)}(\mu) = a_{Mn}^{(qs)}(\mu_0) \left( \frac{\alpha_s(\mu_0)}{\alpha_s(\mu)} \right)^{\gamma_n^{qq}/\beta_0}. \quad (37)$$

We will also take into account the effect of NLO corrections to the DAs. In general, at the NLO the evolution equations for different coefficients  $a_{Mn}^{(q_i)}$  get mixed, and the pattern becomes more complicated. We will consider the NLO evolution for the octet component (see discussion in the next section). The corresponding coefficients evolve according to [39]

$$a_{Mn}^{(qs)\text{NLO}}(\mu) = a_{Mn}^{(qs)}(\mu_0) E_n^{\text{NLO}}(\mu, \mu_0) + \frac{\alpha_s(\mu)}{4\pi} \sum_{k=0}^{n-2} a_{Mk}^{(qs)}(\mu_0) \left( \frac{\alpha_s(\mu_0)}{\alpha_s(\mu)} \right)^{\gamma_k^{qq}/\beta_0} d_n^k(\mu, \mu_0). \quad (38)$$

Explicit expressions for the renormalization factors  $E_n^{\text{NLO}}(\mu, \mu_0)$ , as well as for the off-diagonal mixing coefficients  $d_n^k(\mu, \mu_0)$  in the  $\overline{\text{MS}}$  scheme are collected in Appendix B. Usually the calculation of a few coefficients  $a_{Mn}^{(q_i)}(\mu)$  is sufficient to get a good estimate of the  $\pi$ DA at the scale  $\mu$  from Eq. (29).

### III. DISTRIBUTION AMPLITUDES AND TRANSITION FORM FACTORS IN THE NONLOCAL NJL MODEL

#### A. Quark DAs

From the numerical evaluation of the integrals in Eq. (22) one can obtain the quark DAs for  $\pi$ ,  $\eta$  and  $\eta'$  mesons within the above described three-flavor nlNJL model. The corresponding curves are displayed in Fig. 1, where for comparison we also include the asymptotic limit  $\phi_{\text{asym}}(x) = 6x(1-x)$ .

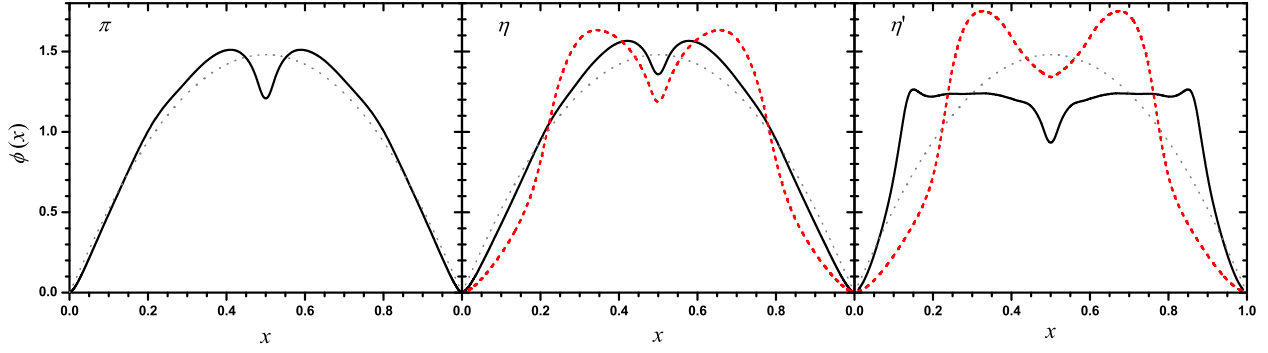


FIG. 1: Quark distribution amplitudes for the  $\pi$ ,  $\eta$  and  $\eta'$  mesons. Left panel:  $\pi$  DA,  $\phi_\pi(x)$ . Central panel:  $\eta$  DAs,  $\phi_\eta^{(q_\ell)}(x)$  (solid line) and  $\phi_\eta^{(q_s)}(x)$  (dashed line). Right panel:  $\eta'$  DAs,  $\phi_{\eta'}^{(q_\ell)}(x)$  (solid line) and  $\phi_{\eta'}^{(q_s)}(x)$  (dashed line). The dotted lines correspond in all cases to the asymptotic limit  $\phi_{\text{asym}}(x) = 6x(1-x)$ .

As stated in the previous section, our calculations have been performed in Euclidean space. The consistency of our procedure has been discussed in Ref. [13], where the pion DA and TFF are analyzed within a two-flavor version of the model. Our main test in this sense is the verification that the sum rule Eq. (6) is satisfied. In the case of  $\eta$  and  $\eta'$  mesons, however, the stringency of this test becomes weakened owing to the numerical uncertainties in the calculations. In fact, when computing the integrals in Eq. (22) one has to take into account that the functions  $F_i(w, x, k_T)$  show cuts in the complex  $w$  plane that require a deformation of the integration paths (see e.g. the discussion in App. B of Ref. [40]). In addition, depending on the value of  $x$  these functions have poles that also need to be compensated numerically. The normalization of quark DAs obtained from our calculations in the present model are 1.0004 for  $\phi_\pi(x)$ , 0.9989 and 0.9753 for  $\phi_\eta^{(q_\ell)}(x)$  and  $\phi_\eta^{(q_s)}(x)$ , respectively, and 1.027 and 0.870 for  $\phi_{\eta'}^{(q_\ell)}(x)$  and  $\phi_{\eta'}^{(q_s)}(x)$ , respectively. It is worth mentioning that the effect of poles and cuts gets increased for higher quark and meson masses, therefore numerical uncertainties are particularly large in the case of the  $s$  quark DA in the  $\eta'$  meson, where we find the largest departure from the normalization condition (the effect of the error in the determination of the  $\eta'$  DAs is discussed above). All quark DAs shown in Fig. 1 have been renormalized so that they satisfy the sum rule.

When using a quark model to describe the deep structure of hadrons it is crucial to establish the chosen scale  $\mu_0$  that will be associated with the results provided by the model. In our case the scale should be the same as that used in lattice calculations, since we have taken into account lattice results in order to fix the shape of the form factors in the quark propagators. Thus, from Ref. [31] we take  $\mu_0 = 3$  GeV, which is a rather large value in comparison with the scale  $\mu_0 \sim 0.5 - 1$  GeV usually adopted in quark model calculations.

In the left panel of Fig. 1 we show the pion DA. Our result is pretty similar to that obtained within

the two-flavor nonlocal NJL model studied in Ref. [13]. Notice that this might not have been the case, since the change from a two-flavor model to the present three-flavor model implies a refitting of all model parameters. By looking at the DAs in Fig. 1 it is seen that in all cases the curves have two symmetric maxima. This is also shown by the  $\pi$  DAs calculated in Refs. [41, 42], albeit in our case the two maxima are much closer to  $x = 0.5$ . In fact, in the nLNJL model this feature arises from the term  $F_i^{(2)}(w, x, k_T)$  [see Eqs. (23-25)], which is a genuine nonlocal contribution. Now, by comparing the curves in the different panels of Fig. 1 one can see the effect of meson and quark masses in the behavior of the DAs. As expected, the  $\pi$  DA at  $\mu_0 = 3$  GeV is relatively close to the asymptotic limit  $\phi_{\text{asym}}(x) = 6x(1-x)$ . This also holds for the  $u$  (or  $d$ ) quark DA in the case of the  $\eta$  meson,  $\phi_{\eta}^{(qe)}(x)$ , while for the strange quark DA  $\phi_{\eta}^{(qs)}(x)$  the deviation from  $\phi_{\text{asym}}(x)$  is more appreciable. Finally, in the case of the  $\eta'$  meson (right panel in Fig. 1), both  $\phi_{\eta'}^{(qe)}(x)$  and  $\phi_{\eta'}^{(qs)}(x)$  lie far from the asymptotic limit. Another important feature, common to all obtained DAs, is that they go to zero rather fast near the points  $x = 0$  and  $x = 1$ , supporting the idea of suppression of the kinematic end points [43, 44].

Let us consider the QCD evolution of the DAs. We recall that we are working within a quark model in which there is no gluon content. Moreover, according to the numerical values of the  $\rho_n^{(\pm)}$  coefficients in Table III (which measure the degree of mixing between quark and gluon components of the DAs in the evolution equations) we can assume the contribution of gluons to be negligible at any  $\mu$  scale. Thus it is possible to use just the octet evolution formulae for all quark DAs. In Tables IV, V and VI we quote the first coefficients of the Gegenbauer expansion obtained from the quark DAs at  $\mu_0 = 3$  GeV in the flavor basis, together with the corresponding values after evolving down to  $\mu = 1$  GeV at NLO. Notice that, in general, within our approach the absolute values of the expansion coefficients  $a_{Mn}^{(qi)}$  decrease rather slowly with  $n$ .

$n$	2	4	6	8	10	12
$a_{\pi n}(3 \text{ GeV})$	-0.0183	-0.0324	0.0048	-0.0090	0.0049	-0.0067
$a_{\pi n}(1 \text{ GeV}) \text{ (NLO)}$	-0.0225	-0.0646	0.0075	-0.0242	0.0114	-0.0205

TABLE IV: Coefficients  $a_{\pi n}$  obtained within the nLNJL model at  $\mu_0 = 3$  GeV, and their values after evolving down to  $\mu = 1$  GeV at NLO.

Our results for the case of the  $\eta$  meson can be compared with those obtained within the (local) Nambu–Jona-Lasinio model in Ref. [28], where only the  $\eta$  meson case is analyzed, since the  $\eta'$  turns out to be unbounded. It is seen that the shapes of the  $\eta$  DAs are quite different from those obtained in the present model, showing only one central maximum (we recall that the origin of the two-maxima behavior shown in Fig. 1 arises from the purely nonlocal contribution). As expected, the differences in the shapes are translated to the coefficients of the Gegenbauer expansion: the first coefficients

$n$	2	4	6	8	10	12
$a_{\eta n}^{(q_l)}(3 \text{ GeV})$	-0.0538	-0.0263	0.0049	-0.0071	0.0033	-0.0049
$a_{\eta n}^{(q_l)}(1 \text{ GeV}) \text{ (NLO)}$	-0.0778	-0.0540	0.0077	-0.0194	0.0071	-0.0152
$a_{\eta n}^{(q_s)}(3 \text{ GeV})$	-0.1185	-0.0577	0.0538	-0.0248	0.0012	0.0023
$a_{\eta n}^{(q_s)}(1 \text{ GeV}) \text{ (NLO)}$	-0.1785	-0.1168	0.1151	-0.0619	0.0016	0.0054

TABLE V: Coefficients  $a_{\eta n}^{(q_l)}$  and  $a_{\eta n}^{(q_s)}$  obtained within the nlNJL model at  $\mu_0 = 3 \text{ GeV}$ , and their values after evolving down to  $\mu = 1 \text{ GeV}$  at NLO.

$n$	2	4	6	8	10	12
$a_{\eta' n}^{(q_l)}(3 \text{ GeV})$	0.1156	-0.0789	-0.0341	0.0023	0.0201	-0.0061
$a_{\eta' n}^{(q_l)}(1 \text{ GeV}) \text{ (NLO)}$	0.1860	-0.1509	-0.0799	0.0019	0.0520	-0.0182
$a_{\eta' n}^{(q_s)}(3 \text{ GeV})$	-0.1343	-0.0568	0.0632	-0.0334	0.0010	0.0104
$a_{\eta' n}^{(q_s)}(1 \text{ GeV}) \text{ (NLO)}$	-0.2031	-0.1155	0.1360	-0.0829	0.0008	0.0291

TABLE VI: Coefficients  $a_{\eta' n}^{(q_l)}$  and  $a_{\eta' n}^{(q_s)}$  obtained within the nlNJL model at  $\mu_0 = 3 \text{ GeV}$ , and their values after evolving down to  $\mu = 1 \text{ GeV}$  at NLO.

obtained in Ref. [28] read  $a_{\eta_2}^{(q_\ell)} = 0.134$ ,  $a_{\eta_4}^{(q_\ell)} = 0.352$ ,  $a_{\eta_2}^{(q_s)} = 0.377$  and  $a_{\eta_4}^{(q_s)} = 0.245$ .

## B. TFFs without gluons

In this subsection we present the results obtained within our approach for the pseudoscalar meson- $\gamma$  TFFs. In fact, we have modified the expression on the right hand side of Eq. (1) by adding subleading terms in an expansion in inverse powers of  $Q^2$ . This procedure has been already used in Refs. [13, 15, 28, 45] in order to account for contributions coming e.g. from higher twist operators. Here we propose to include two terms in this expansion. In addition, let us neglect for now the gluon contribution to the TFFs. This is consistent with a description of mesons within the nlNJL, which has no gluon content. We have in this way

$$Q^2 F_{M\gamma}(Q^2) = \int dx \frac{1}{2} T_{q\bar{q}}(x, Q^2, \mu^2) \Phi_M^{(q)}(x, \mu^2) + \frac{c}{Q^2} + \frac{d}{Q^4}. \quad (39)$$

In accordance with our approximation of neglecting gluon contributions, we will use octet evolution for the whole quark DAs  $\Phi_M^{(q)}(x, \mu^2)$ .

Our results for the  $M$ - $\gamma$  TFFs, where  $M = \pi, \eta$  and  $\eta'$ , are shown in Fig. 2. The curves have been obtained by calculating the corresponding DAs at NLO, using the octet evolution given by Eq. (38). In all cases solid lines correspond to the evaluation of the TFFs under the assumption of no higher twist corrections, i.e. taking  $c = d = 0$ , while dashed lines are obtained from Eq. (39) by

Meson	$c$ (GeV <sup>3</sup> )	$d$ (GeV <sup>5</sup> )	$n$	$\chi^2/n$	$\chi^2/n$ ( $c = d = 0$ )
$\pi$	0.130	-0.234	50	3.9	6.9
$\eta$	0.064	-0.159	30	0.76	1.3
$\eta'$	-0.075	0.049	40	0.88	2.5

TABLE VII: Fitted values of  $c$  and  $d$  for the  $\pi$ -,  $\eta$ - and  $\eta'$ - $\gamma$  TFFs.  $n$  stands for the number of experimental data points in each case. In the last column we quote the value of  $\chi^2$  corresponding to the choice  $c = d = 0$ .

fitting  $c$  and  $d$  to the experimental data. In the case of the  $\pi$ - $\gamma$  and  $\eta$ - $\gamma$  TFFs we have considered all world data, i.e. those obtained by CELLO, CLEO, BaBar and Belle Collaborations for the  $\pi$ - $\gamma$  TFF and those from CLEO and BaBar for the  $\eta$ - $\gamma$  TFF. On the other hand, for the  $\eta'$ - $\gamma$  TFF we have considered only the data from CLEO and BaBar, in view of the large errors in the determination of  $Q^2$  values shown by L3 results (which are also included in the figure). The dotted lines in the graphs correspond to the LO asymptotic  $Q^2 \rightarrow \infty$  limits for the TFFs in QCD, namely

$$Q^2 F_{M\gamma}^{\text{AsymLO}}(Q^2) = \begin{cases} \sqrt{2}f_\pi & M = \pi \\ (\sqrt{2}f_M^8 + 4f_M^0)/\sqrt{3} = (5\sqrt{2}f_M^\ell + 2f_M^s)/3 & M = \eta, \eta' \end{cases} . \quad (40)$$

Finally, the short-dashed curves correspond to what we call the “asymptotic behavior”, obtained from Eq. (39) by taking  $c = d = 0$ , the parton level amplitudes  $T_{q\bar{q}}$  at the NLO, and the asymptotic form of the DAs,  $\Phi_M^{(q)}(x) = \phi_{\text{asym}}(x) = 6x(1-x)$ . One has [8, 36]

$$Q^2 F_{M\gamma}^{\text{AsymNLO}}(Q^2) = \left(1 - 5\frac{\alpha_s(Q^2)}{3\pi}\right) \left[Q^2 F_{M\gamma}^{\text{AsymLO}}(Q^2)\right] . \quad (41)$$

In Table VII we quote the values of  $c$  and  $d$  arising from our fits, together with the number of experimental data considered in each case and the corresponding  $\chi^2$  values. For comparison we also include the  $\chi^2$  obtained when we take  $c = d = 0$ . By looking at the  $\chi^2$  values it is seen that the introduction of higher twist corrections through the  $c$  and  $d$  terms leads to a significant improvement in the theoretical description of the data for both the  $\pi$ - $\gamma$  and  $\eta'$ - $\gamma$  TFFs, while the improvement is not so important in the case of the  $\eta$ - $\gamma$  TFF. In this regard, notice that the better quality of the fits is basically dominated by the description of the low virtuality region (which has less impact in the case of the  $\eta'$ - $\gamma$  TFF owing to the wide dispersion of the data). In fact, by comparing the solid and dashed curves in the figure we observe that in the case of the  $\pi$ - $\gamma$  and  $\eta$ - $\gamma$  TFFs the differences are ruled by the behaviors at  $Q^2 \lesssim 3 \text{ GeV}^2$ , while for the  $\eta'$ - $\gamma$  TFF there is a more steady deviation which covers a region up to  $Q^2 \sim 10 \text{ GeV}^2$ . Moreover, from Table VII it is seen that the signs of  $c$  and  $d$  are the same for  $\pi$ - $\gamma$  and  $\eta$ - $\gamma$  TFFs, whereas they are opposite to those obtained from the fit to  $\eta'$ - $\gamma$  TFF data. This could be related with the octet character of the  $\pi$  and the prevalingly octet character of the  $\eta$ , which contrast with the mostly singlet character of the  $\eta'$ .

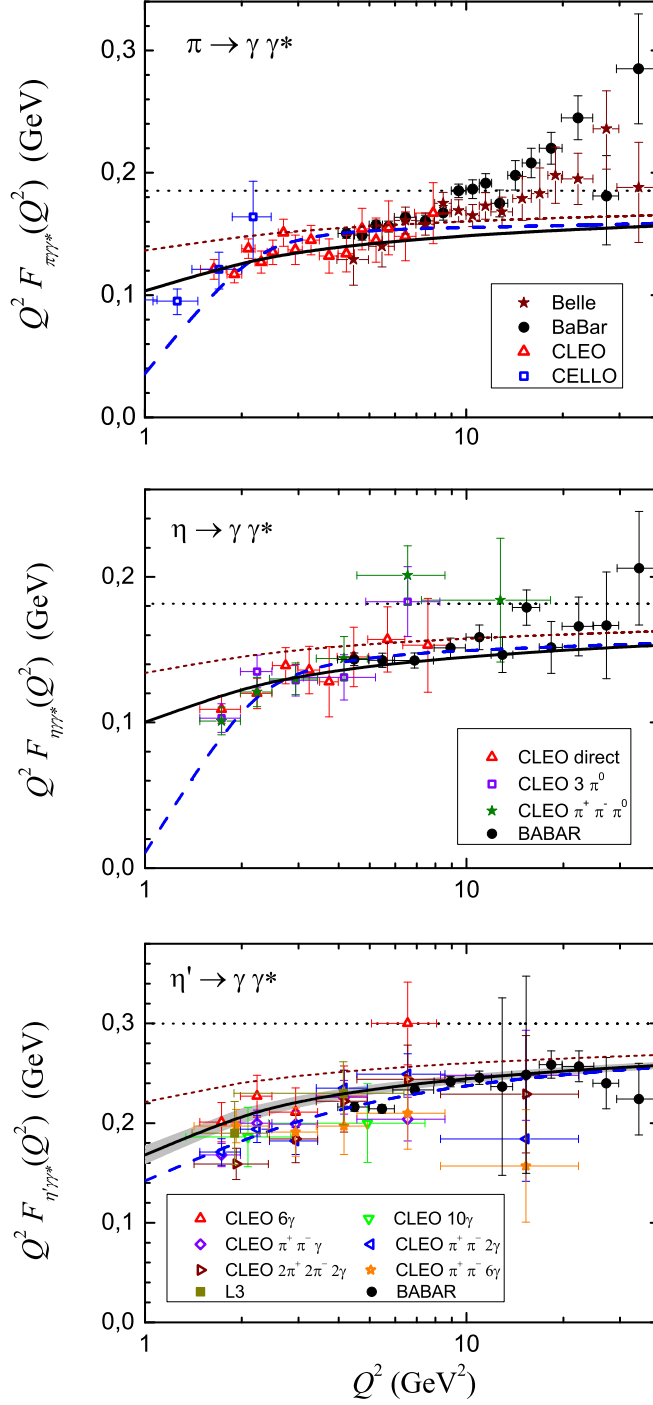


FIG. 2: Theoretical  $\pi$ - $\gamma$ ,  $\eta$ - $\gamma$  and  $\eta'$ - $\gamma$  transition form factors and experimental results from CELLO, CLEO, BaBar, Belle and L3 Collaborations. Solid lines correspond to the case  $c = d = 0$ , while dashed lines correspond to the values of  $c$  and  $d$  in Table VII. Short-dashed lines show the NLO asymptotic QCD behavior (see text), and dotted lines indicate the QCD asymptotic limits. In the case of the  $\eta'$ - $\gamma$  TFF, the gray region corresponds to a change in  $a_{\eta'n}^{(q_i)}$  coefficients within a range of 15%. Notice that in all graphs we have used a logarithmic scale for  $Q^2$ .



Now, while higher twist effects influence the low  $Q^2$  region of the TFFs, it is interesting to analyze the high virtuality region from the point of view of QCD, comparing our results with the asymptotic QCD behavior and the asymptotic limit of the TFFs. From the graphs in Fig. 2 it is seen that in all cases the introduction of NLO corrections to the parton level subprocess amplitudes  $T_{q\bar{q}}$  (while keeping the asymptotic limit for the DAs) has a negative contribution to the TFFs. In addition, it is seen that in all cases the results obtained within the nlNJL model approximate experimental data from below.

Let us comment separately the situation for each meson. In the case of the pion, the experimental data seem to cross the asymptotic limit at some  $Q^2$  value between  $\sim 10 - 20 \text{ GeV}^2$ , hence the NLO corrections go in the wrong direction. This is a well-known problem that we have already discussed in the context of the two-flavor version of the nlNJL model in Ref. [13]. In fact, the puzzling pion data can be described by some models based on flat DAs and some cutoff in the parton amplitudes [15, 45, 46].

In the case of the  $\eta$ - $\gamma$  TFF, even if experimental data for  $Q^2 > 10 \text{ GeV}^2$  seem to follow the asymptotic behavior, the trend of the data shows that it is not unlikely that the TFF crosses the QCD asymptotic limit for higher  $Q^2$  [28]. In any case, according to present experimental results, it can be said that our model provides a good description of the TFF.

Finally, for the  $\eta'$ - $\gamma$  TFF the experimental data lie clearly below the asymptotic behavior, and quite far from the asymptotic QCD limit. Once again the results obtained within the nlNJL model are shown to be in good agreement with the data. Given the uncertainty in the numerical calculations for the  $\eta'$  DA discussed in the previous subsection, we have studied in this case the stability of our results against some variation in the coefficients of the Gegenbauer expansion of the quark DAs. In order to get an estimation of the error we have considered the  $\eta'$ - $\gamma$  TFF for  $c = d = 0$ , allowing for a change in  $a_{\eta'n}^{(q_i)}$  coefficients ( $n \geq 2$ ) within a 15% range. The corresponding range obtained for the TFF is shown by the small gray area in Fig. 2. In general we can state that this error does not affect qualitatively our results.

#### IV. THE EFFECT OF GLUONS

In this section we discuss the possible effect of the presence of gluon components in the DAs. According to the discussion in Sec. II.C, it is natural to carry out our analyses using the octet-singlet basis for the quark distribution amplitudes. At any scale  $\mu$ , we can use Eqs. (28) to obtain the octet and singlet quark DAs from the flavor ones, and analogous expressions can be written for the coefficients of the Gegenbauer expansion. Let us assume that we know the flavor DAs or, equivalently, the coefficients of the Gegenbauer expansion at some scale  $\bar{\mu}_0$ . For the octet and singlet Gegenbauer

coefficients we have

$$\begin{aligned} a_{Mn}^{(qs)}(\bar{\mu}_0) &= \frac{1}{\sqrt{3} f_M^8} \left[ f_M^\ell a_{Mn}^{(q\ell)}(\bar{\mu}_0) - \sqrt{2} f_M^s a_{Mn}^{(qs)}(\bar{\mu}_0) \right], \\ a_{Mn}^{(q0)}(\bar{\mu}_0) &= \frac{1}{\sqrt{3} f_M^0} \left[ \sqrt{2} f_M^\ell a_{Mn}^{(q\ell)}(\bar{\mu}_0) + f_M^s a_{Mn}^{(qs)}(\bar{\mu}_0) \right]. \end{aligned} \quad (42)$$

At LO, the evolution from  $\bar{\mu}_0$  up to a higher scale  $\mu$  is obtained from Eqs. (37) and (32). In particular, for quark singlet and gluon coefficients one has

$$\begin{aligned} a_{Mn}^{(+)}(\bar{\mu}_0) &= \frac{a_{Mn}^{(q0)}(\bar{\mu}_0) - \rho_n^{(-)} a_{Mn}^{(g)}(\bar{\mu}_0)}{1 - \rho_n^{(-)} \rho_n^{(+)}}, \\ a_{Mn}^{(-)}(\bar{\mu}_0) &= \frac{a_{Mn}^{(g)}(\bar{\mu}_0) - \rho_n^{(+)} a_{Mn}^{(q0)}(\bar{\mu}_0)}{1 - \rho_n^{(-)} \rho_n^{(+)}}, \end{aligned} \quad (43)$$

hence

$$\begin{aligned} a_{Mn}^{(q0)}(\mu) &= \frac{1}{1 - \rho_n^{(-)} \rho_n^{(+)}} \left\{ \left[ \left( \frac{\alpha_s(\bar{\mu}_0)}{\alpha_s(\mu)} \right)^{\gamma_n^{(+)} / \beta_0} - \rho_n^{(+)} \rho_n^{(-)} \left( \frac{\alpha_s(\bar{\mu}_0)}{\alpha_s(\mu)} \right)^{\gamma_n^{(-)} / \beta_0} \right] a_{Mn}^{(q0)}(\bar{\mu}_0) \right. \\ &\quad \left. - \rho_n^{(-)} \left[ \left( \frac{\alpha_s(\bar{\mu}_0)}{\alpha_s(\mu)} \right)^{\gamma_n^{(+)} / \beta_0} - \left( \frac{\alpha_s(\bar{\mu}_0)}{\alpha_s(\mu)} \right)^{\gamma_n^{(-)} / \beta_0} \right] a_{Mn}^{(g)}(\bar{\mu}_0) \right\}, \end{aligned} \quad (44)$$

$$\begin{aligned} a_{Mn}^{(g)}(\mu) &= \frac{1}{1 - \rho_n^{(-)} \rho_n^{(+)}} \left\{ \rho_n^{(+)} \left[ \left( \frac{\alpha_s(\bar{\mu}_0)}{\alpha_s(\mu)} \right)^{\gamma_n^{(+)} / \beta_0} - \left( \frac{\alpha_s(\bar{\mu}_0)}{\alpha_s(\mu)} \right)^{\gamma_n^{(-)} / \beta_0} \right] a_{Mn}^{(q0)}(\bar{\mu}_0) \right. \\ &\quad \left. + \left[ \left( \frac{\alpha_s(\bar{\mu}_0)}{\alpha_s(\mu)} \right)^{\gamma_n^{(-)} / \beta_0} - \rho_n^{(+)} \rho_n^{(-)} \left( \frac{\alpha_s(\bar{\mu}_0)}{\alpha_s(\mu)} \right)^{\gamma_n^{(+)} / \beta_0} \right] a_{Mn}^{(g)}(\bar{\mu}_0) \right\}. \end{aligned} \quad (45)$$

In fact, to the order we are working, we should compute the NLO evolution of the DAs. At NLO the evolution of  $a_{Mn}^{(q_i)}(\mu)$  coefficients for different order  $n$  become mixed, as one can see from Eq. (38) for the case of octet components. However, the impact of NLO corrections to the evolution of these coefficients is not significant in comparison with the corresponding corrections for the subprocess amplitudes  $T_{q\bar{q}}$  and  $T_{gg}$  given in Eqs. (2). Indeed, the most important effect on the DAs when going from LO to NLO evolution comes from the change in the strong coupling constant,  $\alpha_s(\mu)$ . Thus we adopt the following prescription: we consider the NLO corrections for  $T_{q\bar{q}}(x, Q^2, \mu^2)$  and  $T_{gg}(x, Q^2, \mu^2)$  [given by Eqs. (2)] together with Eqs. (37) and (44-45) for the evolution of the octet and singlet DAs, respectively. In all these equations we take the NLO running equations for the strong coupling constant  $\alpha_s$ , given by Eq. (64) in App. B. In order to test the validity of this prescription, let us study the case of the octet DAs. In Tables VIII, IX and X we quote the values of the coefficients  $a_{\pi n}$ ,  $a_{\eta n}^{(qs)}$  and  $a_{\eta' n}^{(qs)}$ , respectively, evolved from  $\mu = 3$  GeV to  $\mu = 1$  GeV at LO [i.e., using Eqs. (37) and (63)], at NLO [i.e., using Eqs. (38) and (64)], and within the above described “mixed” approximation, which means to take the LO evolution equation (37) for the coefficients and

$n$	2	4	6	8	10	12
$a_{\pi n}(3 \text{ GeV})$	-0.0183	-0.0324	0.0048	-0.0090	0.0049	-0.0067
$a_{\pi n}(1 \text{ GeV})$ (LO)	-0.0264	-0.0552	0.0091	-0.0187	0.0109	-0.0158
$a_{\pi n}(1 \text{ GeV})$ (NLO)	-0.0225	-0.0646	0.0075	-0.0242	0.0114	-0.0205
$a_{\pi n}(1 \text{ GeV})$ (Mixed)	-0.0284	-0.0614	0.0103	-0.0216	0.0127	-0.0187

TABLE VIII: Coefficients  $a_{\pi n}(\mu)$  obtained within the nlNJL quark model at  $\mu = 3 \text{ GeV}$  and their evolution down to  $\mu = 1 \text{ GeV}$  at LO, at NLO and using the mixed approximation.

$n$	2	4	6	8	10	12
$a_{\eta n}^{(qs)}(3 \text{ GeV})$	-0.0911	-0.0444	0.0331	-0.0173	0.0021	-0.0008
$a_{\eta n}^{(qs)}(1 \text{ GeV})$ (LO)	-0.1315	-0.0758	0.0631	-0.0358	0.0046	-0.0018
$a_{\eta n}^{(qs)}(1 \text{ GeV})$ (NLO)	-0.1357	-0.0902	0.0695	-0.0439	0.0039	-0.0033
$a_{\eta n}^{(qs)}(1 \text{ GeV})$ (Mixed)	-0.1413	-0.0842	0.0716	-0.0414	0.0054	-0.0022

TABLE IX: Coefficients  $a_{\eta n}^{(qs)}(\mu)$  obtained within the nlNJL quark model at  $\mu = 3 \text{ GeV}$  and their evolution down to  $\mu = 1 \text{ GeV}$  at LO, at NLO and using the mixed approximation.

the NLO evolution equation (64) for  $\alpha_s$ . From the values in the tables one can conclude that the “mixed” approximation can be used to estimate NLO calculations with reasonably good accuracy.

We consider here two different ways of estimating the effect of gluons in the DAs. Our first analysis is based on the fact that in general one assumes that the scale at which standard quark models — with no gluon content — can be used to describe hadron physics lies around  $\mu \sim 0.5 - 1 \text{ GeV}$ . Thus, we evolve the quark DAs obtained within the nlNJL from our input scale  $\mu_0 = 3 \text{ GeV}$  to a lower energy scale, which we choose to be  $\bar{\mu}_0 = 0.5 \text{ GeV}$ , and at this lower scale we impose the condition of no gluons. Then, for higher values of  $\mu$ , we allow gluon contributions to be generated through the evolution equations, which mix quark singlet and gluon components of the DAs. For the second analysis, once again we proceed by using the nlNJL quark model parametrization in order to calculate the coefficients  $a_{Mn}^{(q_i)}$  ( $M = \eta, \eta'$ ) of the Gegenbauer expansion of the DAs at the scale  $\mu_0 = 3 \text{ GeV}$ . Now, for  $n \leq \bar{n}$ , where  $\bar{n}$  is some chosen value of  $n$ , we also include nonzero gluon coefficients  $a_{Mn}^{(g)}(\mu_0)$ , and use Eqs. (44) and (45), with  $\bar{\mu}_0 = \mu_0$ , to evolve quark and gluon coefficients to any other scale. The values of the gluon coefficients  $a_{Mn}^{(g)}(\mu_0)$  are then determined from a fit to the experimental data for the TFFs. For the remaining coefficients (those of order  $n > \bar{n}$ ) we proceed in the same way as in the first analysis. The consistency of this approach can be tested by analyzing the stability of the results against changes in the chosen value of  $\bar{n}$ . Notice that this second analysis leads to the presence of gluons at low virtuality, which is compatible with models that include a glueball component for the description of the  $\eta$ - $\eta'$  mixing [47].

$n$	2	4	6	8	10	12
$a_{\eta'n}^{(qs)}(3 \text{ GeV})$	-0.4317	-0.0305	0.1791	-0.0759	-0.0217	0.0301
$a_{\eta'n}^{(qs)}(1 \text{ GeV}) \text{ (LO)}$	-0.6232	-0.0520	0.3418	-0.1577	-0.0483	0.0708
$a_{\eta'n}^{(qs)}(1 \text{ GeV}) \text{ (NLO)}$	-0.6661	-0.0733	0.3930	-0.1839	-0.0601	0.0854
$a_{\eta'n}^{(qs)}(1 \text{ GeV}) \text{ (Mixed)}$	-0.6698	-0.0577	0.3881	-0.1821	-0.0566	0.0837

TABLE X: Coefficients  $a_{\eta'n}^{(qs)}(\mu)$  obtained within the nlNJL quark model at  $\mu = 3 \text{ GeV}$  and their evolution down to  $\mu = 1 \text{ GeV}$  at LO, at NLO and using the mixed approximation.

### A. First analysis

Let us analyze the numerical results obtained for the effect of gluon contributions according to the first analysis proposed above. As stated, we take into account the fact that usually quark models do not include gluons at their scale of validity  $\bar{\mu}_0$ , therefore we can obtain the coefficients  $a_{Mn}^{(q_0)}$  and  $a_{Mn}^{(g)}$  at any scale  $\mu$  from Eqs. (44-45) by imposing  $a_{Mn}^{(g)}(\bar{\mu}_0) = 0$ . Moreover, from Tables II and III it is seen that the values of the  $\rho_n^{(+)}\rho_n^{(-)}$  coefficients are small and the  $\gamma_n^{(+)}$  anomalous dimensions are close to  $\gamma^{qq}$ . Hence we can assume that the mixing with gluons will have small influence on the singlet coefficients  $a_{Mn}^{(q_0)}(\mu)$ . On the other hand, since the values of  $\rho_n^{(+)}$  for low  $n$  are not negligible, the first gluon coefficients  $a_{Mn}^{(g)}(\mu)$  of the Gegenbauer expansion could give some appreciable contribution to  $\eta$  and  $\eta'$  DAs.

As discussed in Sec. II.B, we input the shape of quark propagators at the scale  $\mu_0 = 3 \text{ GeV}$  from lattice QCD calculations. In order to connect the DAs at this scale to those at the lower scale  $\bar{\mu}_0$  that we use as starting point for the QCD evolution we need some approximation. We use here octet evolution, i.e., we begin by considering the calculated DAs at  $\mu_0 = 3 \text{ GeV}$  shown in Fig. 1, and evolve them down to  $\bar{\mu}_0 = 0.5 \text{ GeV}$  assuming no gluon components. Then, starting from the  $\bar{\mu}_0$  scale we use the evolution equations (44-45) to obtain the singlet quark and gluon DAs (the latter, generated by the mixing in the evolution) at any  $\mu$ . Thus at the scale  $\bar{\mu}_0 = 0.5 \text{ GeV}$  we have

$$a_{Mn}^{(g)}(0.5 \text{ GeV}) = 0 ,$$

$$a_{Mn}^{(q_0)}(0.5 \text{ GeV}) = \tilde{a}_{Mn}^{(q_0)}(3 \text{ GeV}) \left[ \frac{\alpha_s(3 \text{ GeV})}{\alpha_s(0.5 \text{ GeV})} \right]^{\gamma_n^{qq}/\beta_0} , \quad (46)$$

where

$$\tilde{a}_{Mn}^{(q_0)}(3 \text{ GeV}) = \frac{1}{\sqrt{3} f_M^0} \left[ \sqrt{2} f_M^\ell a_{Mn}^{(q_\ell)}(3 \text{ GeV}) + f_M^s a_{Mn}^{(q_s)}(3 \text{ GeV}) \right] . \quad (47)$$

The values for the first coefficients  $a_{Mn}^{(q_\ell)}(3 \text{ GeV})$  and  $a_{Mn}^{(q_s)}(3 \text{ GeV})$  for  $M = \eta$  and  $M = \eta'$  are those quoted in Tables V and VI. Notice that when evolving back from  $\mu = \bar{\mu}_0$  to  $\mu = 3 \text{ GeV}$  using the evolution equations (44-45) in general we will obtain a result for  $a_{Mn}^{(q_0)}(3 \text{ GeV})$  different from the input

$n$	2	4	6	8	10	12
$a_{\eta n}^{(q_0)}(1 \text{ GeV})$	0.182	0.107	-0.268	0.094	0.022	-0.066
$a_{\eta n}^{(g)}(1 \text{ GeV})$	0.342	0.062	-0.072	0.014	0.002	-0.004
$a_{\eta' n}^{(q_0)}(1 \text{ GeV})$	-0.022	-0.128	0.036	-0.039	0.027	0.007
$a_{\eta' n}^{(g)}(1 \text{ GeV})$	-0.042	-0.074	0.010	-0.006	0.003	0.0005

TABLE XI: Coefficients  $a_{Mn}^{(q_0)}(\mu)$  and  $a_{Mn}^{(g)}(\mu)$  ( $M = \eta, \eta'$ ) evolved from  $\mu_0 = 0.5 \text{ GeV}$  to  $\mu = 1 \text{ GeV}$  according to our first analysis of gluon contributions.

value  $\tilde{a}_{Mn}^{(q_0)}(3 \text{ GeV})$ . However, since the anomalous dimensions  $\gamma_n^{(+)}$  are close to  $\gamma_n^{qq}$  (see Table II), one expects the differences to be small for all  $n$ .

In Table XI we quote the first coefficients of the Gegenbauer expansion for the quark singlet and gluon DAs at  $\mu = 1 \text{ GeV}$ . As expected from the values of  $\rho_n^{(+)}$  in Table III, it is seen that the coefficients of the gluon DA decrease rapidly with  $n$ . The small value of  $a_{\eta' n}^{(q_0)}$  for  $n = 2$  arises from a cancellation in the r.h.s. of Eq. (47), which reduces significantly the value of  $\tilde{a}_{Mn}^{(q_0)}(3 \text{ GeV})$ .

From our calculations we find that the effect of gluon contributions to the TFFs within this approximation is negligible. In the case of the  $\eta$ - $\gamma$  TFF, the comparison with experimental data for  $c = d = 0$  leads to  $\chi^2/n = 1.33$ , to be compared with the value of 1.30 obtained in absence of gluons (see Table VII). The corresponding curve differs slightly from that plotted in Fig. 2 (central panel, solid line). For the  $\eta'$ - $\gamma$  TFF the influence of gluons in this approximation is also imperceptible. The comparison with data leads to  $\chi^2/n = 2.9$ , somewhat above the value of 2.5 quoted in Table VII, whereas the corresponding curve lies within the uncertainty range indicated by the gray region in the lower panel of Fig. 2.

## B. Second analysis

As stated above, in this second analysis we allow for the presence of nonzero gluon coefficients  $a_{\eta n}^{(g)}$ ,  $a_{\eta' n}^{(g)}$  at a low  $\mu$  scale for  $n \leq \bar{n}$ , where  $\bar{n}$  is some chosen value of  $n$ , and we determine the values of these coefficients by fitting to the experimental data for the  $\eta$ - $\gamma$  and  $\eta'$ - $\gamma$  TFFs. For the coefficients  $a_{Mn}^{(q_0)}$  and  $a_{Mn}^{(g)}$ , with  $n > \bar{n}$ , we proceed as in the first analysis. We consider here the cases  $\bar{n} = 2$  and  $\bar{n} = 4$ , comparing the corresponding numerical results to get an estimation of the stability of the approach.

Let us first take  $\bar{n} = 2$ . In this case we take the coefficients  $a_{Mn}^{(q_0)}$  and  $a_{Mn}^{(g)}$  for  $n \geq 4$  to be the same as those calculated in the previous analysis, therefore the corresponding values at  $\mu = 1 \text{ GeV}$  can be read from Table XI. For the first Gegenbauer coefficients  $a_{\eta 2}^{(q_0)}$  and  $a_{\eta' 2}^{(q_0)}$ , at the scale  $\mu_0 = 3 \text{ GeV}$  we use the input provided by Eq. (42) with  $\bar{\mu}_0 = \mu_0$ , taking the values of  $a_{M2}^{(q_\ell)}(3 \text{ GeV})$  and  $a_{M2}^{(q_s)}(3 \text{ GeV})$

for  $M = \eta, \eta'$  from Tables V and VI. On the other hand, the first gluon coefficients  $a_{\eta 2}^{(g)}$  and  $a_{\eta' 2}^{(g)}$  at the scale  $\mu_0 = 3$  GeV are taken as free parameters to be determined from fits to the  $\eta$ - $\gamma$  and  $\eta'$ - $\gamma$  TFF experimental data, respectively. The theoretical values for the TFFs are obtained by evolving the coefficients  $a_{M 2}^{(q_0)}$  and  $a_{M 2}^{(g)}$  to any scale through the above described “mixed” evolution approximation. Finally we proceed in a similar way, taking now  $\bar{n} = 4$ . Namely, for  $n \geq 6$  we use the same  $a_{M n}^{(q_0)}$  and  $a_{M n}^{(g)}$  coefficients as in the first analysis, we obtain  $a_{M 2}^{(q_0)}(3 \text{ GeV})$  and  $a_{M 4}^{(q_0)}(3 \text{ GeV})$  from Eq. (42) with  $\bar{\mu}_0 = \mu_0$  for  $n = 2$  and  $n = 4$ , respectively, and we determine  $a_{M 2}^{(g)}(3 \text{ GeV})$  and  $a_{M 4}^{(g)}(3 \text{ GeV})$  from fits to the experimental data for the  $\eta$ - $\gamma$  and  $\eta'$ - $\gamma$  TFFs.

To discuss our results we quote not only the values of the coefficients  $a_{M n}^{(q_0)}$  and  $a_{M n}^{(g)}$  obtained at the input scale  $\mu_0 = 3$  GeV but also the corresponding values after the evolution down to 1 GeV, as it is commonly done in the literature. This is especially relevant in this case, since the effect of gluon contributions to the TFFs is more relevant at low virtuality, say  $Q^2 \lesssim 3 \text{ GeV}^2$ . Let us start by analyzing the results for the  $\eta$  meson. From the  $\bar{n} = 2$  fit we obtain  $a_{\eta 2}^{(g)}(3 \text{ GeV}) = 2.66$ , with  $\chi^2/(\text{number of points}) = 1.30$ , while from the  $\bar{n} = 4$  fit we get  $a_{\eta 2}^{(g)}(3 \text{ GeV}) = -109$  and  $a_{\eta 4}^{(g)}(3 \text{ GeV}) = 65.5$ , with  $\chi^2/(\text{number of points}) = 0.71$ . The comparison is more feasible when we evolve the coefficients down to  $\mu = 1$  GeV:

$$\left. \begin{array}{ll} a_{\eta 2}^{(g)}(1 \text{ GeV}) = 6.37 & a_{\eta 2}^{(q_0)}(1 \text{ GeV}) = 0.155 \\ a_{\eta 2}^{(g)}(1 \text{ GeV}) = -275 & a_{\eta 2}^{(q_0)}(1 \text{ GeV}) = 1.24 \\ a_{\eta 4}^{(g)}(1 \text{ GeV}) = 278 & a_{\eta 4}^{(q_0)}(1 \text{ GeV}) = -0.937 \end{array} \right\} \begin{array}{l} \bar{n} = 2 \\ \bar{n} = 4 . \end{array} \quad (48)$$

Taking into account the results of our first analysis (discussed in the previous subsection), in which we obtain  $\chi^2/(\text{number of points}) = 1.33$ , it is seen that the  $\bar{n} = 2$  fit shows no gain of quality in the description of the experimental data. In addition, the  $\bar{n} = 4$  fit leads to a strong cancellation between the  $n = 2$  and  $n = 4$  gluon coefficients. There is no physical reason for this cancellation, therefore we interpret this result as a spurious solution. Thus we conclude that there is no evidence of a significant presence of gluons in the case of the  $\eta$  meson.

For the  $\eta'$  meson the  $\bar{n} = 2$  fit leads to  $a_{\eta' 2}^{(g)}(3 \text{ GeV}) = 4.31$ , while from the  $\bar{n} = 4$  fit we obtain  $a_{\eta' 2}^{(g)}(3 \text{ GeV}) = 4.38$  and  $a_{\eta' 4}^{(g)}(3 \text{ GeV}) = -0.049$ . The quality of the fit is approximately the same in both cases, with  $\chi^2/(\text{number of points}) = 0.91$ . Evolving these coefficients to  $\mu = 1$  GeV we obtain

$$\left. \begin{array}{ll} a_{\eta' 2}^{(g)}(1 \text{ GeV}) = 10.9 & a_{\eta' 2}^{(q_0)}(1 \text{ GeV}) = -0.064 \\ a_{\eta' 2}^{(g)}(1 \text{ GeV}) = 11.1 & a_{\eta' 2}^{(q_0)}(1 \text{ GeV}) = -0.065 \\ a_{\eta' 4}^{(g)}(1 \text{ GeV}) = -0.097 & a_{\eta' 4}^{(q_0)}(1 \text{ GeV}) = -0.127 \end{array} \right\} \begin{array}{l} \bar{n} = 2 \\ \bar{n} = 4 . \end{array} \quad (49)$$

Contrary to the case of the  $\eta$ - $\gamma$  TFF, now we observe that there is a significant gain of quality in the description of the experimental values in comparison with the results from our first analysis and

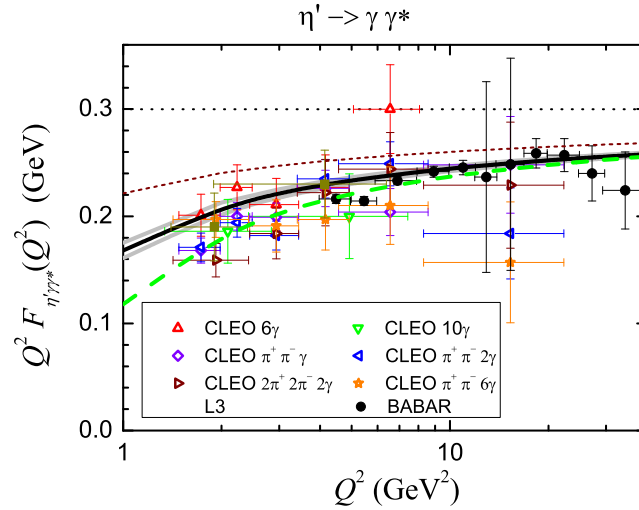


FIG. 3: Theoretical curves and experimental results for the  $\eta'$ - $\gamma$  TFF. The full line corresponds to the NLO result with no gluon contributions discussed in Sec. III, and the gray region indicates the indetermination in the corresponding Gegenbauer coefficients. The dashed line is the TFF obtained when the contributions of gluons are fitted. Short-dashed and dotted lines correspond to the NLO asymptotic behavior of the TFF (see discussion in Sec. III) and the asymptotic limit, respectively. Notice the usage of a logarithmic scale for  $Q^2$ .

with those quoted in Sec. III. We recall that the latter, obtained under the assumption of no gluon contributions to the  $\eta'$  DA, lead to a fit of  $\eta'$ - $\gamma$  TFF with  $\chi^2/n = 2.5$  (see Table VII). Moreover, although the  $\bar{n} = 4$  fit has one more free parameter with respect to the case  $\bar{n} = 2$ , the theoretical description of the  $\eta'$ - $\gamma$  TFF is approximately the same in both cases. Our result is shown by the dashed line in Fig. 3 ( $\bar{n} = 2$  and  $\bar{n} = 4$  fits are indistinguishable). For comparison we also include in the figure the previous NLO result with no gluon contribution (full line, indetermination indicated by the grey band), the “asymptotic behavior”, according to the definition in Sec. III (short-dashed line), and the asymptotic  $Q^2 \rightarrow \infty$  value (dotted line). Our analysis shows that the gluon contribution is sizable in the case of the  $\eta'$  meson. From the figure it is seen that in the low virtuality region the difference between our NLO calculation and the asymptotic behavior is similar to the difference between the present fit and the NLO result. In fact, the result obtained after considering the fitted gluon contributions to the  $\eta'$  DA is comparable to that arising from the inclusion of higher twist contributions, discussed in the previous section.

Finally, it is interesting to compare our results with those obtained in Refs. [19–21]. The authors of these articles perform model independent fits of the  $\eta$ - $\gamma$  and  $\eta'$ - $\gamma$  TFFs, considering only the  $n = 2$  coefficients of the Gegenbauer expansions of the DAs. Moreover, they assume meson independence of the quark and gluon DAs, i.e. they take  $\phi_{\eta}^{(q_i)} = \phi_{\eta'}^{(q_i)}$  and  $\phi_{\eta}^{(g)} = \phi_{\eta'}^{(g)}$ . In this way they end up with only

three free parameters, namely the coefficients  $a_{\eta^{(\prime)2}}^{(qs)}$ ,  $a_{\eta^{(\prime)2}}^{(q0)}$  and  $a_{\eta^{(\prime)2}}^{(g)}$ . The analyses carried out in those papers, considering various fits under different conditions, show that the results are quite stable within the quoted errors. Let us take here as representative values the default results from Ref. [21], namely  $a_{\eta^{(\prime)2}}^{(qs)}(1 \text{ GeV}) = -0.05 \pm 0.02$ ,  $a_{\eta^{(\prime)2}}^{(q0)}(1 \text{ GeV}) = -0.12 \pm 0.01$  and  $a_{\eta^{(\prime)2}}^{(g)}(1 \text{ GeV}) = 19 \pm 5$ , as well as the results in Eq. (63) of Ref. [19], which translated to our notation lead to  $a_{\eta^{(\prime)2}}^{(q0)}(1 \text{ GeV}) = -0.12 \pm 0.11$  and  $a_{\eta^{(\prime)2}}^{(g)}(1 \text{ GeV}) = 18.2 \pm 4.5$ . It is worth noticing that our results do not support the hypothesis of meson independence of quark and gluon DAs, in fact, we find significative differences between them. Nevertheless, it is seen that the values obtained from our analysis are consistent with the above results. Indeed, considering Eq. (3), and taking values of meson decay constants from Table XII, it is seen that the coefficients of  $\phi_M^{(qs)}$  are basically determined by the  $\eta$ - $\gamma$  TFF, whereas those of  $\phi_M^{(q0)}$  (and also  $\phi_M^{(g)}$ ) are mainly fixed by the  $\eta'$ - $\gamma$  TFF. Therefore, the value of  $a_{\eta^{(\prime)2}}^{(qs)}$  in Ref. [21] should be compared with our result in Table IX,  $a_{\eta^2}^{(qs)} = -0.14$ , while the results for  $a_{\eta^{(\prime)2}}^{(q0)}$  and  $a_{\eta^{(\prime)2}}^{(g)}$  in Ref. [21] and Ref. [19] are to be compared with our values  $a_{\eta'^2}^{(q0)} = -0.06$  and  $a_{\eta'^2}^{(g)} = 11$ , see Eq. (49). Taking into account the theoretical and experimental uncertainties, we conclude that the values quoted in Refs. [21] and [19] are compatible with each other and with our results.

## V. CONCLUSIONS

In this work we have evaluated the quark DAs for the  $\eta$  and  $\eta'$  mesons and the associated  $\eta$ - $\gamma$  and  $\eta'$ - $\gamma$  TFFs within the framework of a nonlocal Nambu–Jona-Lasinio model. This approach, which has been shown to provide a successful description of various meson observables [30, 35], has been previously considered in Ref. [13] for the study of the  $\pi$  meson DA and the  $\pi$ - $\gamma$  TFF. Since the theoretical framework satisfies all basic symmetry requirements (i.e. chiral, Poincaré and local electromagnetic gauge invariances), the quark DAs turn out to be naturally normalized within this scheme.

One of the main ingredients of our model is the quark propagator, which by construction shows a momentum dependence consistent with lattice QCD results. The calculated quark DAs have to be therefore associated to the momentum scale of lattice data, namely 3 GeV [31]. In general, the comparison of any observable related to the quark DAs (as e.g. the  $M$ - $\gamma$  TFF) with experimental data will require a perturbative evolution of the results obtained at this reference scale. Here we have carried out this evolution up to NLO accuracy in  $\alpha_s$ , neglecting the mixing between Gegenbauer coefficients of different orders for the singlet quark and gluon DAs.

From the obtained quark DAs at the scale of 3 GeV we observe the following features: (i) whereas our  $\pi$ DA is not far from the asymptotic distribution  $\phi_{\text{asym}}(x) = 6x(1-x)$ , the  $\eta$  and  $\eta'$  quark DAs move away from the asymptotic behavior, the departure being larger the larger the meson mass is;



(ii) all DAs show two maxima, and this structure arises from the nonlocal genuine contributions in Eq. (25); (iii) in all cases the DAs go to zero rather fast near  $x = 0$  and  $x = 1$ , supporting the idea of suppression of the kinematic end points [43, 44]. Another outcome of our results is that when the DAs are expanded in Gegenbauer polynomials we find that the absolute values of the corresponding coefficients decrease rather slowly with  $n$ , in contrast with usual assumptions.

Concerning the evaluation of the  $M\text{-}\gamma$  TFFs, we have found that in general NLO corrections lead to a suppression of  $Q^2 F(Q^2)$ . Although this represents a problem regarding the explanation of the already challenging experimental scenario for the  $\pi\text{-}\gamma$  TFF, the corrections go in the right direction in the case of the  $\eta\text{-}\gamma$  and  $\eta'\text{-}\gamma$  TFFs. An important difference between the case of the  $\pi$  meson and those of the  $\eta$  and  $\eta'$  mesons is that  $\eta$  and  $\eta'$  states can include a gluon-gluon component. In this regard, we have firstly performed an analysis in which these gluon components have been neglected for all  $Q^2$  values, while higher twist corrections have been taken into account by adding  $1/Q^2$  and  $1/Q^4$  terms to the dominant twist 2 contribution provided by the DAs. Then we have fitted these contributions to  $M\text{-}\gamma$  TFF data. From our results it is seen that the effect of higher twist corrections is more important for the  $\pi\text{-}\gamma$  and  $\eta\text{-}\gamma$  TFFs, particularly for  $Q^2 \lesssim 3 \text{ GeV}^2$ . Moreover, it is seen that the signs of the corresponding contributions are the same in both cases. Conversely, for the  $\eta'\text{-}\gamma$  TFF, contrary to what it should be expected, the higher twist corrections appear to be less concentrated in the low virtuality region.

Finally, we have investigated the effect of two-gluon components of the  $\eta$  and  $\eta'$  mesons to leading-twist accuracy, considering NLO perturbative QCD and neglecting the mixing between Gegenbauer coefficients of different orders. From the numerical analysis it is found that the evolution equations do not generate an appreciable contribution if we assume that meson DAs include no gluons at low virtuality. On the other hand, if we allow for the presence of gluon-gluon components in the  $\eta$  and  $\eta'$  DAs at low momentum scales, it is seen that the experimental data for the corresponding TFFs suggest an important gluon component in the  $\eta'$  state and a less important one in the  $\eta$  state. According to the discussion in Sec. IV.B, our results for the first Gegenbauer coefficients of quark DAs at the scale of 1 GeV are

$$\begin{aligned} a_{\eta 2}^{(qs)}(1 \text{ GeV}) &= -0.14 & a_{\eta 4}^{(qs)}(1 \text{ GeV}) &= -0.08 \\ a_{\eta 2}^{(q0)}(1 \text{ GeV}) &= 0.18 & a_{\eta 4}^{(q0)}(1 \text{ GeV}) &= 0.11 \\ a_{\eta' 2}^{(qs)}(1 \text{ GeV}) &= -0.67 & a_{\eta' 4}^{(qs)}(1 \text{ GeV}) &= -0.06 \\ a_{\eta' 2}^{(q0)}(1 \text{ GeV}) &= -0.06 & a_{\eta' 4}^{(q0)}(1 \text{ GeV}) &= -0.13 \end{aligned}$$

For the gluon DAs, our results in the case of the  $\eta$  meson are not conclusive, whereas for the  $\eta'$  we obtain

$$a_{\eta' 2}^{(g)}(1 \text{ GeV}) = 11 \quad a_{\eta' 4}^{(g)}(1 \text{ GeV}) = -0.10$$

As discussed in Sec. IV.B, these results are found to be compatible with previous fits for Gegenbauer coefficients quoted in Refs. [19–21]. In this way, from our analysis we conclude that  $\pi$ - $\gamma$  and  $\eta$ - $\gamma$  TFFs are more sensible to corrections coming from higher twist effects, while the experimental data on the  $\eta'$ - $\gamma$  TFF points to the presence of a significant gluon-gluon component in the  $\eta'$  state.

## Acknowledgments

We thank Prof. S. Scopetta for interesting discussions. This work has been partially funded by CONICET (Argentina) under grants No. PIP 578 and PIP 449, by ANPCyT (Argentina) under grants No. PICT-2011-0113 and PICT-2014-0492, by the National University of La Plata (Argentina), Project No. X718, by the Mineco (Spain) under contract FPA2013-47443-C2-1-P, by the Centro de Excelencia Severo Ochoa Programme, grant SEV-2014-0398, and by Generalitat Valenciana (Spain), grant PrometeoII/2014/066. DGD acknowledges financial support from CONICET under the PVCE programme D2392/15.

## Appendix A: Details of the model

In this appendix we provide some details on the calculation of the quark DAs in Eq. (22). We start from the Euclidean action in Eq. (10), to which we add a coupling with an external axial gauge field  $\mathcal{A}_\mu^a$ , as described in Sec. II.B. Then we perform a standard bosonization of the fermionic theory, introducing scalar fields  $\sigma_a(x)$ ,  $\zeta(x)$  and pseudoscalar fields  $\pi_a(x)$ , together with auxiliary fields  $S_a(x)$ ,  $P_a(x)$  and  $R(x)$ , with  $a = 0, \dots, 8$ . Details of this procedure can be found e.g. in Ref. [30]. As in that work, we use the stationary phase approximation, replacing the path integral over the auxiliary fields by the corresponding argument evaluated at the minimizing values  $\tilde{S}_a(x)$ ,  $\tilde{P}_a(x)$ , and  $\tilde{R}(x)$ . This leads to the equations

$$\begin{aligned}\sigma_a(x) + G \tilde{S}_a(x) + \frac{H}{2} A_{abc} \left[ \tilde{S}_b(x) \tilde{S}_c(x) - \tilde{P}_b(x) \tilde{P}_c(x) \right] &= 0, \\ \pi_a(x) + G \tilde{P}_a(x) + H A_{abc} \tilde{S}_b(x) \tilde{P}_c(x) &= 0, \\ \zeta(x) + G \tilde{R}(x) &= 0.\end{aligned}\tag{50}$$

Thus the bosonized action can be written as

$$\begin{aligned}S_E^{\text{bos}} &= -\ln \det \mathcal{D} + \int d^4x \left\{ \sigma_a(x) \tilde{S}_a(x) + \pi_a(x) \tilde{P}_a(x) + \zeta(x) \tilde{R}(x) \right. \\ &\quad + \frac{G}{2} \left[ \tilde{S}_a(x) \tilde{S}_a(x) + \tilde{P}_a(x) \tilde{P}_a(x) + \tilde{R}(x)^2 \right] + \\ &\quad \left. + \frac{H}{4} A_{abc} \left[ \tilde{S}_a(x) \tilde{S}_b(x) \tilde{S}_c(x) - 3 \tilde{S}_a(x) \tilde{P}_b(x) \tilde{P}_c(x) \right] \right\},\end{aligned}\tag{51}$$

where

$$\begin{aligned} \mathcal{D} \left( y + \frac{z}{2}, y - \frac{z}{2} \right) = & \gamma_0 W \left( y + \frac{z}{2}, y \right) \gamma_0 \left\{ \delta^{(4)}(z) \left( -i\not{p} + m_c \right) \right. \\ & \left. + \left[ \mathcal{G}(z) \left[ \sigma^a(y) + i\gamma_5 \pi^a(y) \right] \lambda^a + \mathcal{F}(z) \sigma_2(y) \frac{i\overleftrightarrow{\not{p}}}{2\kappa_p} \right] \right\} W \left( y, y - \frac{z}{2} \right). \end{aligned} \quad (52)$$

As usual, we assume that, owing to parity conservation and charge and isospin symmetries, the fields  $\sigma^a(x)$ ,  $a = 0, 8$ , and  $\zeta(x)$  have nontrivial translational invariant mean field values  $\bar{\sigma}^a$  and  $\bar{\zeta}$ , while mean field values of the remaining fields are zero. Thus we write

$$\begin{aligned} \sigma_a(x) &= \bar{\sigma}_a + \delta\sigma_a(x), \\ \pi_a(x) &= \delta\pi_a(x), \\ \zeta(x) &= \bar{\zeta} + \delta\zeta(x). \end{aligned} \quad (53)$$

Replacing in the bosonized effective action, and expanding the latter in powers of meson fluctuations  $\xi$  and powers of the gauge field  $\mathcal{A}_\mu^a$ , we obtain

$$S_E^{\text{bos}} = S^{(\text{MFA})} + S^{(\xi^2)} + S^{(\xi\mathcal{A})} + \dots, \quad (54)$$

where only the terms relevant for our calculation have been explicitly written.

The mean field action per unit volume reads

$$\begin{aligned} \frac{S^{(\text{MFA})}}{V^{(4)}} = & 2N_c \sum_f \int \frac{d^3p}{(2\pi)^3} \log \left[ \frac{Z(p)^2}{p^2 + M_f(p)^2} \right] \\ & - \left( \bar{\zeta} \bar{R} + \frac{G}{2} \bar{R}^2 + \frac{H}{4} \bar{S}_u \bar{S}_d \bar{S}_s \right) - \frac{1}{2} \sum_f \left( \bar{\sigma}_f \bar{S}_f + \frac{G}{2} \bar{S}_f^2 \right), \end{aligned} \quad (55)$$

where we have rotated neutral fields from the  $\text{SU}(3)_F$  basis to a flavor basis,  $\sigma_a, \pi_a \rightarrow \sigma_f, \pi_f$ , where  $a = 0, 3, 8$  and  $f = u, d, s$ , or equivalently  $f = 1, 2, 3$ . The functions  $M_f(p)$  and  $Z(p)$  correspond to the momentum-dependent effective masses and WFR of quark propagators introduced in Sec. II.B [see Eqs. (13) and (14)], while  $\bar{S}_f$  and  $\bar{R}$  stand for the values of the fields  $\tilde{S}_f(x)$  and  $\tilde{R}(x)$  within the MFA, respectively. The minimization of  $S^{(\text{MFA})}$  with respect to  $\bar{\sigma}_f$  and  $\bar{\zeta}$  leads to the corresponding Schwinger-Dyson equations [30].

The piece of the bosonic Euclidean action that is quadratic in the meson fluctuations can be written as

$$S_E^{(\xi^2)} = \frac{1}{2} \int \frac{d^4p}{(2\pi)^4} \sum_M r_M G_M(p^2) \xi_M(p) \bar{\xi}_M(-p), \quad (56)$$

where meson fluctuations  $\delta\sigma_a, \delta\pi_a$  have been translated to a charge basis  $\xi_M$ ,  $M$  being the scalar and pseudoscalar mesons in the lowest mass nonets ( $\sigma, \pi^0$ , etc.), plus the  $\zeta$  field. The coefficient  $r_M$  is 1 for charge eigenstates  $M = a_0^0, \sigma, f_0, \zeta, \pi^0, \eta, \eta'$ , and 2 for  $M = a_0^+, K_0^{*+}, K_0^{*0}, \pi^+, K^+, K^0$ .

The full expressions for the one-loop functions  $G_M(q)$ , as well as those for the above mentioned Schwinger-Dyson equations, can be found in Ref. [30]. Meson masses can be obtained by solving the equations

$$G_M(-m_M^2) = 0. \quad (57)$$

In order to obtain physical states  $\tilde{\xi}_M$  one still has to introduce a wave function renormalization factor,

$$\tilde{\xi}_M(p) = Z_M^{-1/2} \xi_M(p), \quad (58)$$

where

$$Z_M^{-1} = \left. \frac{dG_M(p)}{dp^2} \right|_{p^2=-m_M^2} = g_{Mqq}^{-2}. \quad (59)$$

Finally, the bilinear piece in  $\xi_M$  and  $\mathcal{A}_\mu^a$  fields in Eq. (54) is given by

$$S_E^{(\xi\mathcal{A})} = \text{Tr} [\mathcal{D}_0^{-1} \mathcal{D}_\xi \mathcal{D}_0^{-1} D_{\mathcal{A}}] - \text{Tr} [\mathcal{D}_0^{-1} \mathcal{D}_{\xi\mathcal{A}}], \quad (60)$$

where  $\mathcal{D}_\xi$ ,  $\mathcal{D}_{\mathcal{A}}$  and  $\mathcal{D}_{\xi\mathcal{A}}$  stand for the terms in the expansion of Eq. (52) that are linear in  $\xi_M$  and/or  $\mathcal{A}_\mu^a$ . Then the meson DAs within the nlNJL model can be obtained by taking the functional derivative of  $S^{(\xi\mathcal{A})}$  with respect to  $\xi_M$  and  $\mathcal{A}_\mu^a$ . The corresponding expressions are lengthy, and will not be quoted here. After some work one arrives at the result in Eqs. (22- 27).

It is worth noticing that, owing to the bilocal character of the current in Eq. (4), one gets an extra delta function that involves the + components of the momenta. Namely, if  $\Gamma$  represents some operator that includes dirac and flavor matrices, one has

$$\int \frac{dz^-}{2\pi} \bar{\psi}\left(-\frac{z}{2}\right) \Gamma \psi\left(\frac{z}{2}\right) \Big|_{z^+=0, \bar{z}_T=0} e^{iP^+z^-(x-\frac{1}{2})} = \quad (61)$$

$$\int \frac{d^4p_1}{(2\pi)^4} \frac{d^4p_2}{(2\pi)^4} \delta\left(P^+\left(x - \frac{1}{2}\right) - \frac{p_1^+ + p_2^+}{2}\right) \bar{\psi}_{p_2} \Gamma \psi_{p_1}. \quad (62)$$

The numerical results for meson masses and weak decay constants obtained within the present nonlocal model, taking the parameters in Table I, are listed in Table XII.

	$m_\pi$ (MeV)	$m_K$ (MeV)	$m_\eta$ (MeV)	$m_{\eta'}$ (MeV)	$f_\pi$ (MeV)	$f_K/f_\pi$	$f_\eta^0/f_\pi$	$f_\eta^8/f_\pi$	$f_{\eta'}^0/f_\pi$	$f_{\eta'}^8/f_\pi$
Model	139*	495*	523	958*	92.4*	1.17	0.209	1.085	1.496	-0.463
Empirical	139	495	547	958	92.4	1.22	0.187	1.174	1.155	-0.456

TABLE XII: Numerical results from our model and empirical values for various phenomenological quantities. Input values are indicated with an asterisk.

## Appendix B: NLO renormalization factors for the QCD evolution of the octet DA

We quote here the expressions for the renormalization factors  $E_n^{\text{NLO}}$  and  $d_n^k$  needed to calculate the evolution of the coefficients  $a_{Mn}(\mu)$  in Eq. (38). One has

$$E_n^{\text{NLO}}(\mu, \mu_0) = \left( \frac{\alpha_s(\mu_0)}{\alpha_s(\mu)} \right)^{\gamma_n^{qq}/\beta_0} \left[ 1 + \frac{\alpha_s(\mu) - \alpha_s(\mu_0)}{8\pi} \frac{\gamma_n^{qq}}{\beta_0} \left( \frac{\gamma_n^{(1)}}{\gamma_n^{qq}} - \frac{\beta_1}{\beta_0} \right) \right],$$

where  $\beta_0$  ( $\beta_1$ ) and  $\gamma_n^{qq}$  ( $\gamma_n^{(1)}$ ) are the LO (NLO) coefficients of the QCD  $\beta$ -function and the anomalous dimensions, respectively. One has  $\beta_1 = 102 - 38 n_f/3$ , where  $n_f$  is the number of flavors (we take here  $n_f = 4$ ). The values of  $\beta_0$  and  $\gamma_n^{qq}$  are given in Sec. II C, and analytical expressions for  $\gamma_n^{(1)}$  can be found in Refs. [48, 49]. For the evolution of the strong coupling constant  $\alpha_s$  at LO we use

$$\alpha_s(\mu) = \frac{4\pi}{\beta_0 \ln(\mu^2/\Lambda^2)}, \quad (63)$$

with  $\Lambda = 0.224$  GeV, while at NLO we take

$$\alpha_s(\mu) = \frac{4\pi}{\beta_0 \ln(\mu^2/\Lambda^2)} \left\{ 1 - \frac{\beta_1}{\beta_0^2} \frac{\ln[\ln(\mu^2/\Lambda^2)]}{\ln(\mu^2/\Lambda^2)} \right\}, \quad (64)$$

with  $\Lambda = 0.326$  GeV.

On the other hand, the off-diagonal mixing coefficients  $d_n^k$  in Eq. (38) are given by

$$d_n^k(\mu, \mu_0) = \frac{M_n^k}{\gamma_n^{qq} - \gamma_k^{qq} - 2\beta_0} \left\{ 1 - \left[ \frac{\alpha_s(\mu)}{\alpha_s(\mu_0)} \right]^{\gamma_n^{qq} - \gamma_k^{qq} - 2\beta_0 / 2\beta_0} \right\}. \quad (65)$$

Here the matrix elements  $M_n^k$  are defined as

$$M_n^k = \frac{(k+1)(k+2)(2n+3)}{(n+1)(n+2)} [\gamma_n^{qq} - \gamma_k^{qq}] \\ \times \left\{ \frac{8C_F A_n^k - \gamma_k^{qq} - 2\beta_0}{(n-k)(n+k+3)} + 4C_F \frac{A_n^k - S_1(n+1)}{(k+1)(k+2)} \right\}, \quad (66)$$

where

$$A_n^k = S_1 \left( \frac{n+k+2}{2} \right) - S_1 \left( \frac{n-k-2}{2} \right) + 2 S_1(n-k-1) - S_1(n+1), \quad (67)$$

with

$$S_1(n) = \sum_{j=1}^n \frac{1}{j}. \quad (68)$$

Numerical values of the coefficients  $M_n^k$  for  $n \leq 12$  can be found in Ref. [39].

[1] A. J. Bevan *et al.* [BaBar and Belle Collaborations], Phys. J. C **74**, 3026 (2014).

[2] B. Aubert *et al.* [BABAR Collaboration], Phys. Rev. D **80**, 052002 (2009).

- [3] S. Uehara *et al.* [BELLE Collaboration], Phys. Rev. D **86**, 092007 (2012).
- [4] P. del Amo Sanchez *et al.* [BABAR Collaboration], Phys. Rev. **D84**, 052001 (2011).
- [5] J. Gronberg *et al.* [CLEO Collaboration], Phys. Rev. D **57**, 33 (1998).
- [6] M. Acciarri *et al.* [L3 Collaboration], Phys. Lett. B **418**, 399 (1998).
- [7] H. J. Behrend *et al.* [CELLO Collaboration], Z. Phys. C **49**, 401 (1991).
- [8] G. P. Lepage and S. J. Brodsky, Phys. Rev. D **22**, 2157 (1980).
- [9] A. V. Efremov and A. V. Radyushkin, Phys. Lett. B **94**, 245 (1980).
- [10] T. Zhong, X. G. Wu and T. Huang, Eur. Phys. J. C **76**, 390 (2016).
- [11] H. N. Li, Y. L. Shen and Y. M. Wang, JHEP **1401**, 004 (2014).
- [12] J. P. B. C. de Melo, B. El-Bennich and T. Frederico, Few Body Syst. **55**, 373 (2014).
- [13] D. Gomez Dumm, S. Noguera, N. N. Scoccola and S. Scopetta, Phys. Rev. D **89**, 054031 (2014).
- [14] X. G. Wu, T. Huang and T. Zhong, Chin. Phys. C **37**, 063105 (2013).
- [15] S. Noguera and V. Vento, Eur. Phys. J. A **48**, 143 (2012).
- [16] N. G. Stefanis, A. P. Bakulev, S. V. Mikhailov and A. V. Pimikov, Nucl. Phys. Proc. Suppl. **225-227**, 146 (2012).
- [17] N. G. Stefanis, A. P. Bakulev, S. V. Mikhailov and A. V. Pimikov, Phys. Rev. D **87**, 094025 (2013).
- [18] G. F. de Teramond and S. J. Brodsky, arXiv:1203.4025 [hep-ph].
- [19] S. S. Agaev, N. G. Stefanis, Phys. Rev. D **70**, 054020 (2004).
- [20] P. Kroll and K. Passek-Kumericki, Phys. Rev. D **67**, 054017 (2003).
- [21] P. Kroll and K. Passek-Kumericki, J. Phys. G **40**, 075005 (2013).
- [22] S. S. Agaev, V. M. Braun, N. Offen, F. A. Porkert and A. Schäfer, Phys. Rev. D **90**, 074019 (2014).
- [23] R. Escribano, P. Masjuan and P. Sanchez-Puertas, Phys. Rev. D **89**, 034014 (2014).
- [24] R. Escribano, P. Masjuan and P. Sanchez-Puertas, Eur. Phys. J. C **75**, 414 (2015).
- [25] Y. Klopot, A. Oganesian and O. Teryaev, Phys. Rev. D **87**, 036013 (2013); Erratum: [Phys. Rev. D **88**, 059902 (2013)].
- [26] H. Czyz, S. Ivashyn, A. Korchin and O. Shekhovtsova, Phys. Rev. D **85**, 094010 (2012).
- [27] C. Q. Geng and C. C. Lih, Phys. Rev. C **86**, 038201 (2012); Erratum: [Phys. Rev. C **87**, 039901 (2013)].
- [28] S. Noguera and S. Scopetta, Phys. Rev. D **85**, 054004 (2012).
- [29] A. Scarpettini, D. Gomez Dumm and N. N. Scoccola, Phys. Rev. D **69**, 114018 (2004).
- [30] J. P. Carlomagno, D. Gomez Dumm and N. N. Scoccola, Phys. Rev. D **88**, 074034 (2013).
- [31] M. B. Parappilly, P. O. Bowman, U. M. Heller, D. B. Leinweber, A. G. Williams and J. B. Zhang, Phys. Rev. D **73**, 054504 (2006).
- [32] P. O. Bowman, U. M. Heller, and A. G. Williams, Phys. Rev. D **66**, 014505 (2002); P. O. Bowman, U. M. Heller, D. B. Leinweber and A. G. Williams, Nucl. Phys. Proc. Suppl. **119**, 323 (2003).

- [33] S. Noguera, Int. J. Mod. Phys. E **16**, 97 (2007).
- [34] S. Noguera and V. Vento, Eur. Phys. J. A **28**, 227 (2006).
- [35] S. Noguera and N. N. Scoccola, Phys. Rev. D **78**, 114002 (2008).
- [36] F. del Aguila and M. K. Chase, Phys. B **193**, 517 (1981).
- [37] E. Braaten, Phys. Rev. D **28**, 524 (1983).
- [38] R. D. Bowler and M. C. Birse, Nucl. Phys. A **582**, 655 (1995); R. S. Plant and M. C. Birse, Nucl. Phys. A **628**, 607 (1998).
- [39] S. S. Agaev, V. M. Braun, N. Offen and F. A. Porkert, Phys. Rev. D **83**, 054020 (2011).
- [40] M. F. Izzo Villafañe, D. Gomez Dumm and N. N. Scoccola, Phys. Rev. D **94**, 054003 (2016).
- [41] V. L. Chernyak and A. R. Zhitnitsky, Nucl. Phys. B **201**, 492 (1982); Erratum: [Nucl. Phys. B **214**, 547 (1983)]; Phys. Rept. **112**, 173 (1984).
- [42] A. P. Bakulev, S. V. Mikhailov and N. G. Stefanis, Lett. B **508**, 279 (2001); Erratum: [Phys. Lett. B **590**, 309 (2004)].
- [43] S. V. Mikhailov and N. G. Stefanis, Nucl. Phys. B **821**, 291 (2009).
- [44] S. V. Mikhailov, A. V. Pimikov and N. G. Stefanis, Phys. Rev. D **82**, 054020 (2010).
- [45] S. Noguera and V. Vento, Eur. Phys. J. A **46**, 197 (2010).
- [46] A. V. Radyushkin, Phys. Rev. D **80**, 094009 (2009).
- [47] V. Mathieu and V. Vento, Phys. Rev. D **81**, 034004 (2010).
- [48] A. Gonzalez-Arroyo, C. Lopez and F. J. Yndurain, Nucl. Phys. B **153**, 161 (1979).
- [49] E. G. Floratos, D. A. Ross and C. T. Sachrajda, Nucl. Phys. B **129**, 66 (1977); Erratum: [Nucl. Phys. B **139**, 545 (1978)].